99 11

CONDUCTION PROPERTIES OF BORON DOPED POLYCRYSTALLINE-SILICON FILMS

By

MUKESH RANJAN

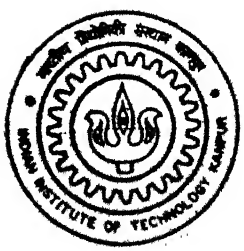

NUCLEAR ENGINEERING AND TECHNOLOGY PROGRAMME

Indian Institute of Technology Kanpur

JULY, 2001

CONDUCTION PROPERTIES OF BORON DOPED POLYCRYSTALLINE-SILICON FILMS

A Thesis Submitted

In Partial Fulfillment of the Requirements

For the Degree of

Master of Technology

By

Mukesh Ranjan

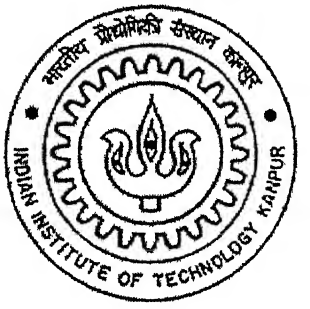

Nuclear Engineering and Technology Programme

Indian Institute Of Technology Kanpur

JULY 2001

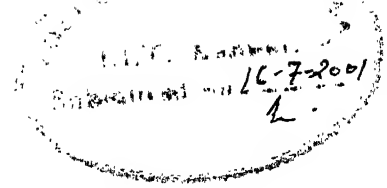

CERTIFICATE

It is certified that the work contained in the thesis entitled "**Conduction Properties of Boron Doped Polycrystalline-Silicon Films**", by Mukesh Ranjan, has been carried out under my supervision and that this work has not been submitted elsewhere for a degree.

13/7/2001

Dr. S. Qureshi
Professor,
Nuclear Engineering and Technology Programme
Indian Institute of Technology Kanpur
July 2001

Abstract

Study of the electronic properties namely conductivity, mobility and dominant transport mechanism across the grain boundaries, in case of boron doped polycrystalline-silicon films, was carried out in this work. The study shows that the average carrier concentration varies with the level of boron dopant concentration in the material. While at high dopant concentration most of the dopants contribute to average carriers, the average carrier concentration at low doping concentration is only a small fraction of the dopant concentration. This phenomenon is attributed to the presence of grain boundary traps in material .the study shows that at Boron dopant concentration of $10^{14}cm^{-3}$, the free carrier concentration for 200A° and 1220A° grain size material is approximately $10^{9}cm^{-3}$ The study also shows that at lower dopant concentration ($<10^{17}cm^{-3}$) thermionic emission (TE) is the dominant mechanism behind carrier transport across the grain boundaries. However, both thermionic emission (TE) and thermionic field emission with scattering (TFES) contribute to carrier transport at high dopant concentration (10^{17}-$10^{18}cm^{-3}$). Further, at very high doping concentration, TFES is the dominant mechanism of transport across the grain boundaries.

Acknowledgement

I wish to express my deep sense of gratitude to Dr. S. Qureshi, for his excellent guidance and all round assistance at every stage of my work. I also express my sincere gratitude to Mr. M.J. Siddiqui, for his valuable guidance and moral support throughout, which led to successful completion of this work.

I also owe thanks to Dr. Prabhat Munshi for always being supportive to me. His help, academically and otherwise, is gratefully acknowledged.

Special thank to my friends Priyanshu Goel & Ritesh Chauresia for their academic support.

I would always remember the company of my friends Vineet, Ajay, Suneet, Deba, Hemant and Shailesh for their lively company and co-operation throughout my tenure of my stay at IIT Kanpur.

The love, caring and constant encouragement from my parents are invaluable assets that I got throughout the course of study. Without them nothing would have been possible.

Mukesh Ranjan

Contents

List of Figures

List of Tables

Nomenclature

E_C	Energy of the conduction band edge
E_F	Fermi level energy
h	Plank's constant
J	Current density
k	Boltzmann constant
L	Average total length of a grain
L_g	Width of the undepleted portion of the grain
L_{gb}	Width of the composite grain boundary region
m_h^*	Effective mass of the hole
N	Doping concentration
N_G	Average dopant concentration in the grains
q	Charge of hole
Q_t	Density of carrier trapping states at grain boundaries
T	Measurement temperature (^{0}K)
V_b	Height of the potential barrier in the depletion region
V_o	Voltage drop across the composite grain-boundary region
V_a	Average voltage drop across a grain
V_L, V_R	Voltage drops across the depletion region on the left and right sides of the grain boundary, respectively
V_d	Half of the voltage drop across the depletion region
W	Width of depleted region
W_{gb}	Grain-boundary width
ξ	Fermi level relative to edge of conduction band
σ	Average conduction
σ_{gb}	Conductivity of the grain boundary

ρ	Average resistivity
ρ_{gb}	Resistivity of grain boundary
ϕ	Height of the grain-boundary barrier relative to E_V
ϕ_{gb}	Height of the grain-boundary relative to E_F
$D(E_x)$	Tunneling probability in the x-direction of the carrier.
$D_{LR}(E_x)$, $D_{RL}(E_x)$	Tunneling probability from left to right & right to left respectively
$f(E)$	Fermi function
p_x, p_y, p_z	Respectively, the component of momentum in the x, y,& z direction
$N(\xi,E,T)$	The number of carrier having energy within the range dE_x incident on the barrier per second per unit area
N_{LR}, N_{RL}	The number of hole tunneling from left to right and right to left, respectively.
TFES	Thermionic field emission with the scattering from the grain boundary barrier
TE	Thermionic emission.

Chapter 1

Introduction

Polysilicon has many important applications in integrated-circuit technology. Heavily doped polycrystalline -silicon films are commonly used as the gate electrodes and interconnections in silicon-gate MOS integrated circuits. Lightly doped films are frequently used for high value resistors in static memory circuits. Large gain polysilicon has the potential for the large volume production of low cost solar cells. In the past years, particular attention has been given to polycrystalline -silicon films and their application in microelectronics.

Because of the wide applications of polycrystalline -silicon in integrated circuit technology, its electrical properties have been the focus of increasing attention by many researchers. These investigations have shown that electrical properties of polycrystalline -silicon are markedly different from those of single crystal silicon. At low dopant concentration the resistivity is several orders of magnitude higher than that of single crystal silicon and is not sensitive to change in the dopant concentration .At medium dopant concentration a small increase in dopant concentration results in a sharp drop in the resistivity. At high dopant concentrations the resistivity approaches that of single crystal silicon, although it always remains slightly higher.

This high resistivity of lightly doped polycrystalline -silicon has been utilized in various applications such as high value load resistors in static RAM's.

During the last two decades, a significant amount of work concerning the various properties of un doped or doped polysilicon films at different annealing temperature was done. Most of the work was oriented towards phosphorous – doped polysilicon films used as the gate material in metal oxide semiconductor (MOS) technology and to arsenic –doped polysilicon mainly used as the emitter contacts in bipolar technology. Polycrystalline -silicon thin-film transistors (poly-Si TFT) have been studied because of their potential application in high – performance active matrix liquid crystal displays (AMLCD).

Much less attention has been given to boron-doped polysilicon especially at low dopant concentration, which is now commonly used in the state of the art silicon self –aligned bipolar technology as the extrinsic base contact. Boron doped polysilicon has drawn considerable attention for its potential application in polysilicon devices namely n-channel thin film transistors (TFTS). Therefore, a better knowledge of its conduction properties is necessary for proper design of the device.

In the present work a model based on a combination of, carrier trapping and carrier Tunneling at grain boundary is used to explain the electrical conduction in B-doped polysilicon. To Study the dominant mechanism of transport at different doping levels analytical calculation is done first and then the results are compared with the experimental results known from various references. Calculated results accurately predict the conduction properties of polycrystalline - silicon films as a function of dopant concentration. Special interest is shown to calculate free carrier concentration at very low doping concentration ($<10^{16}cm^{-3}$).
The report is organized in remaining five chapters with the following contents:
Chapter 2 summarizes some basic definitions and theories, which are used as tools in the following chapters.
In **Chapter 3** analytical calculations of the transport properties, resistivity and mobility have been done.

In **Chapter 4** numerical calculations of grain boundary width and results obtained are shown and a comparison is made with the experimental results.

In **Chapter 5** analysis and discussion of the results are given.

Chapter 6 gives the conclusions and further scope to improve the results.

Chapter 2

Models for Conduction in Polysilicon

2.1 Polysilicon Grain & Grain Boundary

In the single crystal silicon, dopant impurities diffuse in to the perfect lattice structure by interacting with point defects, such as silicon vacancies and interstitials. A polycrystalline material is composed of small crystal lattices joined together by grain boundaries. Inside each crystallite the atoms are arranged in a periodic manner so that it can be considered, as a small single crystal .The grain boundary is a complex structure, usually consisting of a few atomic layers of disordered atoms (Figure-1a -1b). In case of polysilicon, two silicon crystals are connected through the grain boundaries alternatively. Like open crystal structure associated with the dangling bonds at dislocations allows rapid dopant migration along the dislocations, likewise in the polysilicon grain boundaries disorder ness provides high diffusivity paths along which dopant atoms can easily move. Even though the grain boundaries occupy only a small fraction of the sample volume, dopant migration along these path can markedly increase the over all dopant diffusion in the polysilicon.

The dopant diffusion depends strongly on the crystal structure of the polysilicon as well as the detailed structure of the grain boundaries. Although the dopant atoms are not electrically active while they are in the grain boundary after diffusing along the grain boundary, they can move back into the grain and influence the electrical properties of the polysilicon. Grain boundary is a thin region of high diffusivity, normal to the sample surface between the two grains of

low diffusivity. Enhanced diffusion associated with the grain boundary can be described as a two -step process, the dopant atom first diffuses rapidly along the disordered structure of the grain boundary and then moves laterally into the grain, where it diffuses less rapidly.

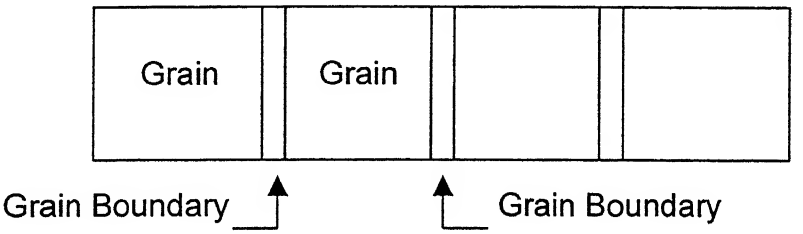

Figure 1a: Grains and Grain Boundaries

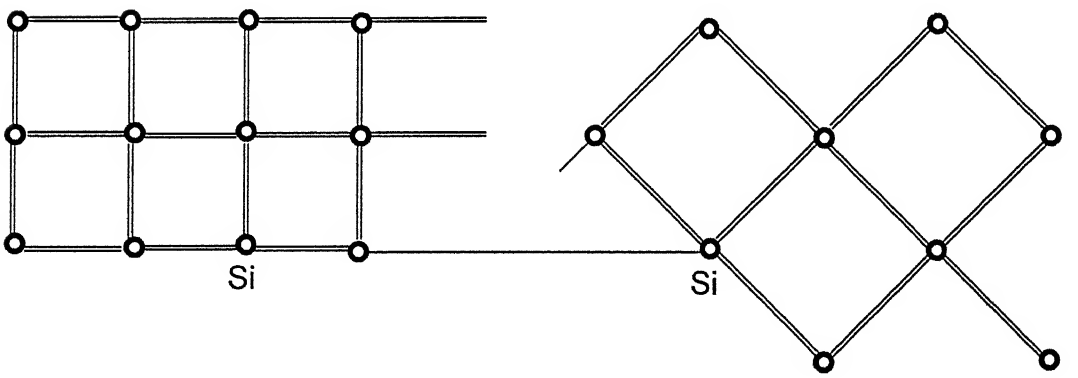

Figure 1b: Dangling bonds at the grain boundary

2.2 Models for Conduction Mechanism in Polysilicon

At low dopant concentrations, polycrystalline -silicon is characterized by a resistivity much higher than that of single crystal silicon, with low sensitivity to changes in dopant concentration [1] - [7]. At medium dopant concentration, a small increase in the dopant concentration cause a sharp drop in the resistivity. At high dopant concentration, the resistivity approaches that of single-crystal

silicon, although it always remains slightly higher (Figure-2). On the other hand, carrier mobility in polycrystalline -silicon is lower than carrier mobility in single-crystal silicon through out the whole dopant concentration range and is characterized by a minimum value at an intermediate dopant concentration [1] to [4].

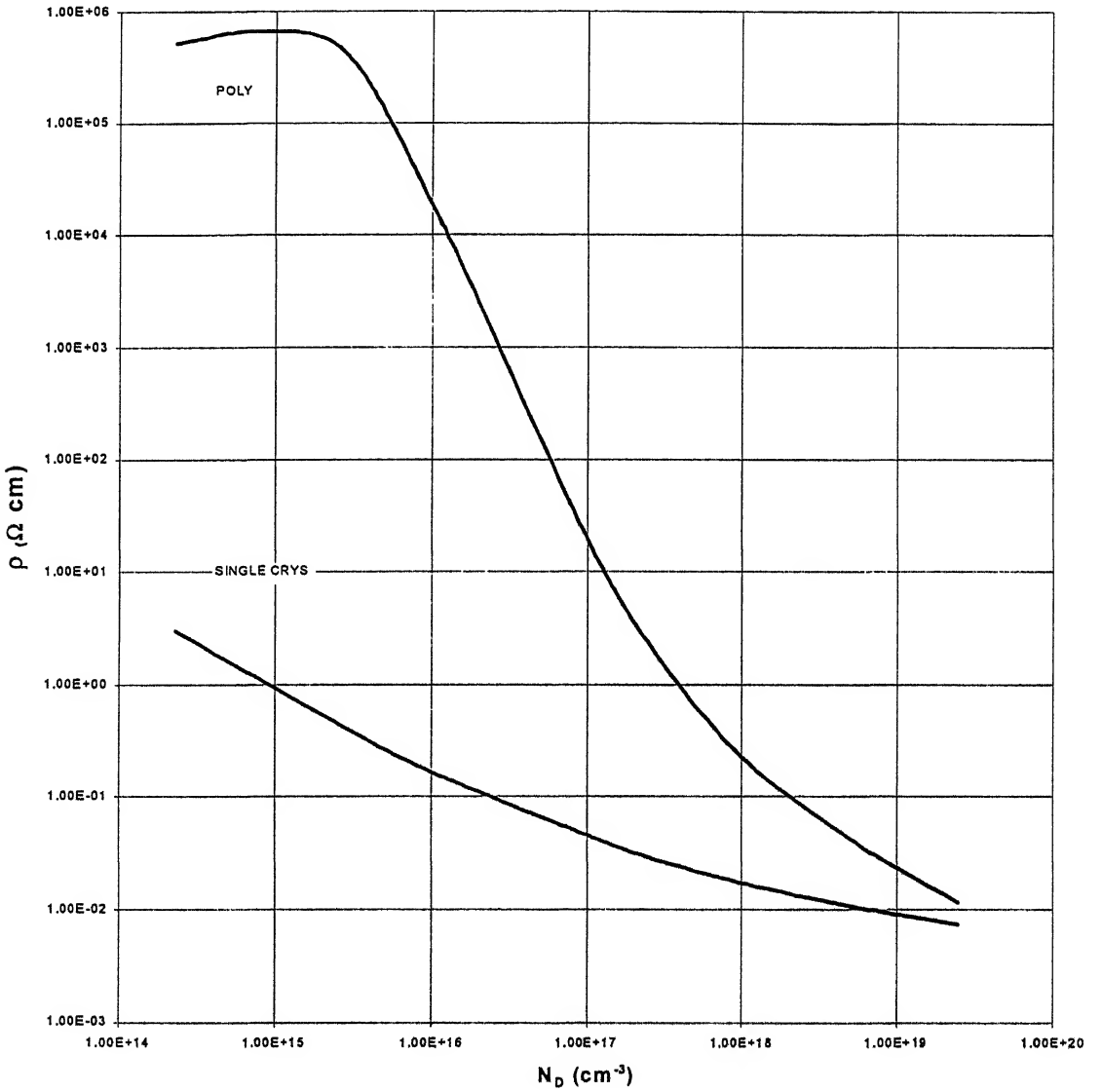

Figure 2: Comparison of Polysilicon and Single Crystal resistivity

Several models have been proposed to explain the resistivity variation with dopant concentration in polycrystalline -silicon. In the present work following three models have been used:

(i) The carrier –trapping model

(ii) The dopant-segregation model

(iii) The modified model

Each model explains the electrical properties of polycrystalline -silicon.

2.2.1 The Carrier-Trapping Model

This model postulates that the dopant atoms are uniformly distributed through out the material and that conductivity is limited by carrier trapping at the grain boundaries, where the trapped carriers create potential barriers, which impede the transport of free carriers between the grains [1] - [7],[20] and [28].

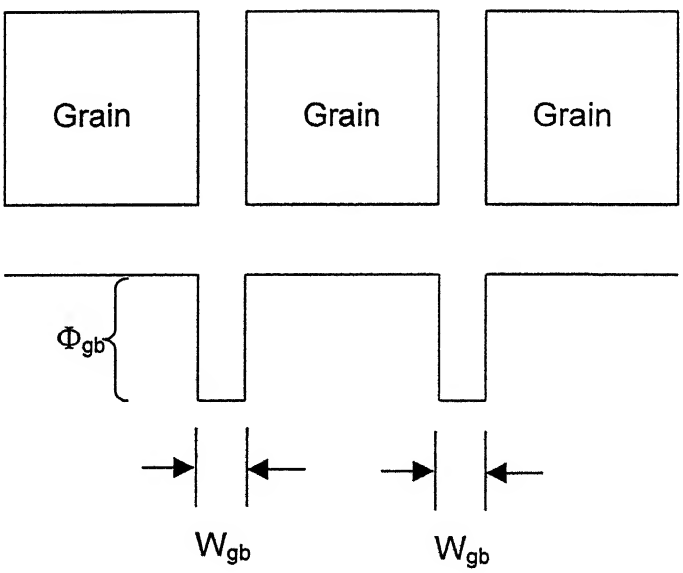

Figure 3: A schematic representation of potential barriers

The high resistivity observed at low dopant concentrations is explained by the trapping of most of the carriers at the grain boundaries, leaving few free to contribute to the conduction. As the dopant concentration is increased, the number of the trapped carriers increases and eventually approaches saturation.

Upon further increase in dopant concentration, the number of trapped carriers does not increase appreciably; consequently, the potential barriers decrease, resulting in a sharp reduction in resistivity [1,4]. Finally, at high dopant concentrations, the potential barrier at the grain boundaries become very small and no longer limit the conductivity of the samples and the properties of the materials approach those of the grains.

The reason behind carrier trapping is that since the atoms at the grain boundary are disordered, there are a large number of defects due to incomplete atomic bonding. This results in the formation of trapping state. These trapping states are capable of trapping carriers and thereby immobilize them. This reduces the number of free carriers available for electrical conduction. After the mobile carrier is trapped the trap becomes electrically charged, creating a potential energy barrier, which impedes the motion of the carriers from one grain to the neighboring grain, there by reducing their mobility. Based on this model, for the same amount of doping, the mobility & carrier concentration of a polycrystalline semiconductor would be less than that of a single crystalline material.

2.2.2 Dopant Segregation Model

In this model grain boundary acts as sink for impurity atoms due to impurity segregation at the grain boundary. Consequently the amount of impurity in the crystallite is reduced, which leads to a much smaller carrier concentration than the uniformly distributed impurity concentration. The carrier concentration does not approach that of the doping concentration until the grain boundary is saturated with impurity atoms. It is also suggested that segregation of impurity caused the grain interior to have higher resistance than the grain boundaries [18]. It has been shown that segregation of boron at the grain boundary is significant only at extremely heavily doped concentration of silicon. No segregation was observed for doping as high as 1.3×10^{20} cm^{-3} [2],[7], [8] & [24]. If the reduction

of carriers is the result of impurity segregation at the grain boundary, it is expected that the carrier concentration reduction would depend on the impurity element. It was observed that both boron & phosphorous behaved similarly in polysilicon.

In this model variation in the resistivity is explained by the hypothesis that low dopant concentration most of the atoms segregate to the grain boundaries, leaving few to contribute to conduction. As the dopant concentration is increased, more atoms remain inside the grains, and thus the resistivity approaches that of single –crystal silicon.

Although both the models were successful in explaining the variation of resistivity with total dopant concentration, the carrier-trapping model has been more generally accepted because the dopant segregation model cannot explain either the temperature dependence of the film resistivity or the minimum in Hall mobility observed at intermediate dopant concentration [4]. However, neither the trapping model nor the segregation model predict any dependence of the electrical properties on the high–temperature processing or on the type of dopant species.

2.2.3 Modified Model

In this model [4], as the atoms are arranged in a periodic manner forming small single crystal, while the grain boundaries are composed of disordered atoms & contain large number of defects due to incomplete bonding. The high concentration of the defects and dangling bonds at the grain boundaries is the origin of the trapping states and the dopant segregation sites around which the carrier trapping and dopant segregation model were developed [1] to [9],[20]. In these model the grain boundary regions have always been assumed to be very narrow compared to the size of the crystallites, thus only the effect of the

Segregation sites and trapping states at the grain boundaries on the number of active dopant atoms and free carriers have been taken into consideration. However, due to highly disordered nature of the grain boundaries and the fact that they introduce discontinuities in the otherwise periodic single –crystal nature of the crystallites, they should be expected to play an additional direct role in determining conduction mechanism in the carriers.

In order to model the effect of the grain boundaries on the Electrical properties of polycrystalline -silicon, some basic assumptions about the properties of the grain boundaries have to be made.

The nature of the grain boundary material can be considered to be between that of a completely ordered single crystal and that of highly disordered amorphous material. The optical energy gap of amorphous silicon has been measured by many researchers [14] -[16], [25] -[27] and was found to be about 1.5 –1.6 eV, much larger than the energy gap of single-crystal silicon. Therefore, the energy gap of the grain boundary material can be expected to be somewhat larger than the energy gap of the single –crystal material within the crystallite.

The high concentration of defects and dangling bonds at the grain boundaries provide ideal sites at which each donor dopant atom at the gain boundary could have all of its five bond saturated. Similarly, the three bonds of an acceptor atom could be accommodated. Consequently, the dopant atoms at the grain boundaries have no weekly bound carriers, and the Fermi level is pinned near mid gap at the gain boundaries [14-15] and [28-30].

As a result of the above assumption, a hetero-junction is formed at the interface between a crystallite and a grain boundary, with the grain boundary material behaving as intrinsic wide –band-gap semiconductor. Therefore the effect of the grain boundaries can be modeled by potential barriers, shown in Figure –(4).

behaving as intrinsic wide –band-gap semiconductor. Therefore the effect of the grain boundaries can be modeled by potential barriers, shown in Figure –(4).

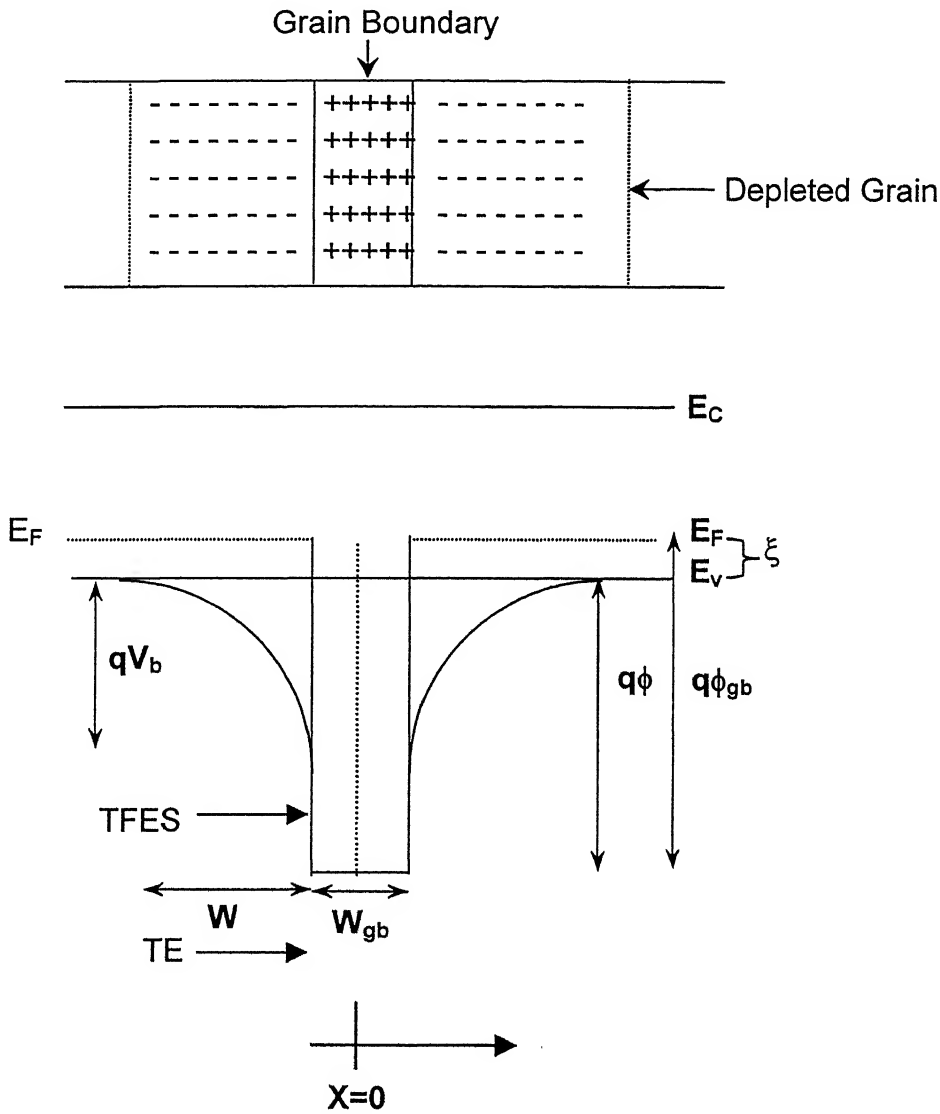

Figure 4: Energy band diagram for zero applied voltage

The height of this barrier $q\phi_{gb}$, relative to the Fermi level, is equal to $E_{gb}/2$,where E_{gb} is the band gap of the grain boundary material, and the width of each of

these potential barriers W_{gb} is approximately equal to the width of the grain boundary. Thus in orders to move from one crystallite to other the carriers have to either tunnel through the barrier or be sufficiently energetic to be thermally emitted over the barrier.

The potential energy in the depletion region $qV(x)$ relative to the valence band edge E_V in the neutral region of the grain is given as a function of distance x by reference [1], [2], [4] and [20]. (Appendix A)

$$qV(x) = \frac{q^2.N}{2\varepsilon}\left[\left(W + \frac{W_{gb}}{2}\right) - |x|\right]^2 \quad ; \text{ For } \frac{W_{gb}}{2} < |x| < \left(W + \frac{W_{gb}}{2}\right)$$

Which has the maximum value qV_b given by,

$qV_b = \frac{q^2 N W^2}{2\varepsilon}$, For the completely depleted region $W = 2L$

$$qV_b = \frac{q^2 N L^2}{8\varepsilon} \quad ; \quad \text{For } LN < Q_t \qquad \text{(a)}$$

$$qV_b = \frac{q^2 Q_t^2}{8\varepsilon N} \quad ; \text{For } LN < Q_t \qquad \text{(b)}$$

2.3 W.K.B Method

The grain boundary material has a resistivity much higher than that of the grains due to its intrinsic and highly disordered nature. Thus conduction mainly takes place by carrier motion from one grain to another by tunneling though and/or by thermionic emission over the barriers at grain boundary.

The one-dimensional time –dependent tunneling probability D (E_x) for a barrier of height qV (x) is given in the W.K.B approximation using references [11-12]

$$D(E_x) = \exp\left\{\frac{-4\pi}{h}\int_a^b \left[2m_h^*(qV(x) - E_x)\right]^{\frac{1}{2}} dx\right\}$$

Where E_x is the energy component of the incident carrier in the X-direction with zero energy taken at the top of the valence band in the neutral region of the grains, and m_h^*, the effective mass of the carriers is assumed to be energy independent. (Appendix-B). The validity of the W.K.B tunneling probability approximation has been studied theoretically and experimentally by [17,39], and was found that. Polysilicon satisfies all the conditions (small grain boundary width, depletion potential and grain boundary potential) shown in [39] to use W.K.B technique.

2.4 Fermi-Dirac Statistics

Fermi-Dirac statistics give the distribution of the holes having energy E by the following equation.

$$N(E) = [1 - f(E)]\bar{w}$$

$$N(E) = \bar{w}\left(1 - \frac{1}{\left[1 + \exp\frac{(E - E_F)}{kT}\right]}\right) \quad ;$$

Where E_F is the Fermi energy & $\bar{w}$ is the weight factor. Above equation show the number of holes [13].

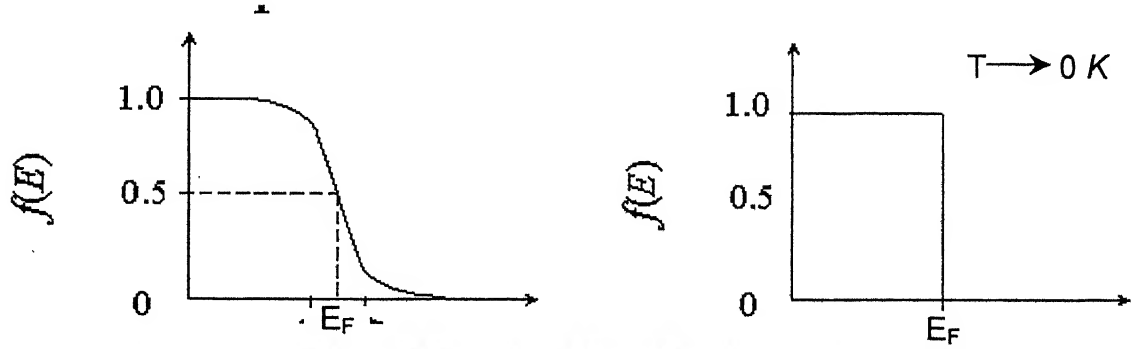

Chapter 3

Analytical Calculations

3.1 Hole Density Incident On The Barrier

For the calculations of the current density (J) the hole density incident on the barrier per unit area & per unit time is required. To calculate hole density Fermi-Dirac statistics is used, according to which, out of N holes $N(E_r)$ are in the state E_r and weight $\bar{w}$ is given by

$$N(E) = \bar{w}\left(1 - \frac{1}{\left[1 + \exp\frac{(E - E_F)}{kT}\right]}\right) \tag{1a}$$

Or

$$N(E) = \bar{w}\left(\frac{1}{\left[1 + \exp\frac{(E_F - E)}{kT}\right]}\right) \tag{1b}$$

In the phase space-weighting factor is given by, [14]& [19].

$$\bar{w} = \frac{2V}{h^3} dp_x dp_y dp_z \tag{2}$$

Here V is the volume in spatial coordinates i.e. $V = dxdydz$

From equation (1) and (2),

$$N(E_{x,y,z}) = \frac{2V dp_x dp_y dp_z}{h^3} \left(\frac{1}{\left[1 + \exp \frac{(E_F - E)}{kT} \right]} \right) \tag{3}$$

Number of holes moving in x-direction in range dp_x per unit area and time,

$$N(E_x) = \frac{2p_x dp_x}{h^3 m_h^*} \int_{-\infty}^{\infty} dp_y \int_{-\infty}^{\infty} \left(\frac{1}{\left[1 + \exp \frac{(E_F - E)}{kT} \right]} \right) dp_z \tag{4}$$

The total kinetic energy E_r in the x-direction is given by

$$E_r = \frac{1}{2m_h^*} \left(p_x^2 + p_y^2 + p_z^2 \right) \tag{5}$$

Solving these equation using polar co-ordinates in *Y-Z* plane

$$\begin{aligned} &\therefore p_y^2 + p_z^2 = p_\rho^2 \\ &dp_y dp_z = p_\rho dp_\rho d\theta \end{aligned} \tag{6}$$

So the equation become (4)

$$N(E_x) = \frac{2p_x dp_x}{h^3 m_h^*} \int_0^{2\pi} \int_0^{\infty} \frac{p_\rho dp_\rho d\theta}{\left[1 + \exp - \left(\frac{\left(p_x^2 + p_\rho^2 \right)}{2m_h^* kT} - \frac{E_F}{kT} \right) \right]} \tag{7}$$

And its solution is given by,

$$N(E_x) = \frac{4\pi}{h^3} kT p_x dp_x \ln \left\{ 1 + \exp \frac{\left(\frac{p_x^2}{2m_h^*} - E_F \right)}{kT} \right\}$$

Converting the equation in terms of energy and taking the hole kinetic energy w.r.t valence band.

$$N(\xi,E_x,T)=\frac{4\pi}{h^3}m_h^* kT \ln\left\{1+\exp\frac{-(E_x+\xi)}{kT}\right\}dE_x \tag{8}$$

Where $\xi=E_F-E_V$.

This is the final expression of the hole density entering at the potential barrier per unit time, per unit area (Appendix-C)

3.2 Current Density (J) Produced By Charge Carriers

Let V_0 be the voltage drop across the complete grain boundary region. This will be drop in voltage across the grain –boundary. Barrier and the two depletion regions on either side of the grain boundary, are as shown in the Figure -(6) such that.

$$V_o=V_{gb}+V_L+V_R \tag{9}$$

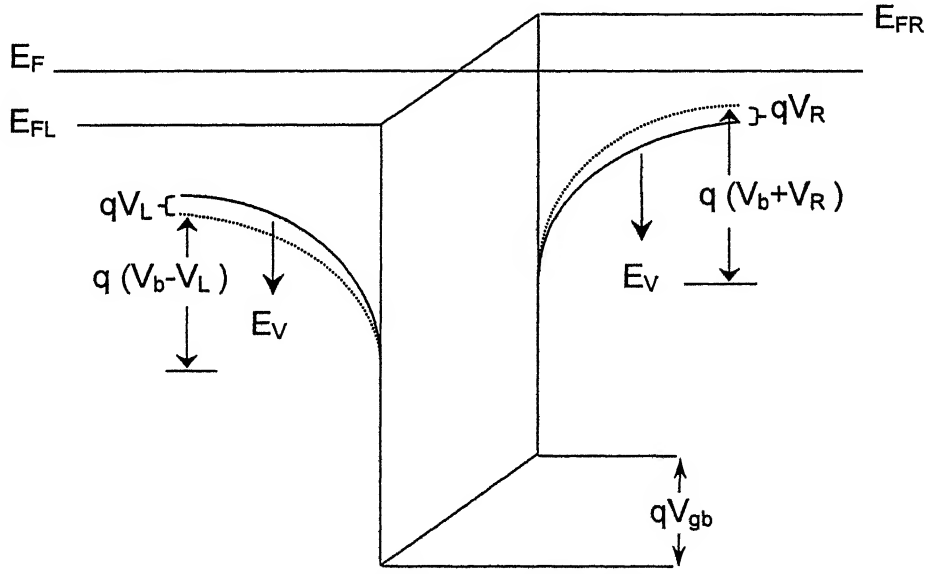

Figure 6: Energy band diagram near a grain boundary at an applied voltage

Now the number of electrons tunneling from left to right N_{LR} and number of electron tunneling from right to left N_{RL} can be calculated by integrating $D(E_x)N(\xi,E_x,T)$ over all energies & using (2.3) with equation (8).

$$\left.\begin{aligned} N_{LR} &= \frac{4\pi}{h^3} m_h^* kT \int_0^\infty \ln\left\{1+\exp\left[\frac{-\left(E_x+\xi-\frac{qV_{gb}}{2}-qV_L\right)}{kT}\right]\right\} D_{LR}(E_x)dE_x \\ N_{RL} &= \frac{4\pi}{h^3} m_h^* kT \int_0^\infty \ln\left\{1+\exp\left[\frac{-\left(E_x+\xi+\frac{qV_{gb}}{2}+qV_R\right)}{kT}\right]\right\} D_{RL}(E_x)dE_x \end{aligned}\right\} \quad (10)$$

In general D_{LR} (E_X) and D_{RL} (E_X) are function of different voltages dropped across the grain boundary regions on its sides so that $D_{LR}(E_X) \neq D_{RL}(E_X)$.

Thus the net current density (J) through the grain boundary is given by

$J = q\,[N_{LR} \sim N_{RL}]$

So putting the N_{LR} and N_{RL} from equation (10) we get,

$$J = q\left(\frac{4\pi}{h^3} m_h^* kT\right)\left[\int_0^\infty \ln\left\{1+\exp\left[\frac{-\left(E_x+\xi-\frac{qV_{gb}}{2}-qV_L\right)}{kT}\right]\right\} D_{LR}(E_x) - \int_0^\infty \ln\left\{1+\exp\left[\frac{-\left(E_x+\xi+\frac{qV_{gb}}{2}+qV_R\right)}{kT}\right]\right\} D_{RL}(E_x)\right] dE_x \quad (11)$$

Now to solve equation (11), we need tunneling probabilities $D_{LR}(E_X)$ and $D_{RL}(E_X)$, both of which depend on barrier $qV(x)$. From the Figure it is clear that $qV(x)$ can have different forms depending on the energy of the carriers.

So we have three different conditions.

(i) $E_x<qV(x)$ (TFE): For the carriers, which have energies less than the energy required to over come the potential barrier in the depleted regions of the grains, the potentials barrier qV (x) is defined as follows,

$$\left.\begin{aligned} qV(x) &= 0 && for\,|x| > W + W_{gb}/2 \\ qV(x) &= \frac{q^2 N}{2\varepsilon}\left[\left(W + W_{gb}/2\right) - |x|\right]^2 && for\, W_{gb}/2 < |x| < W + W_{gb}/2 \\ qV(x) &= q\phi && for\,|x| < W_{gb}/2 \end{aligned}\right\} \quad (12)$$

In this case thermionic field emission is possible (TFE)

(ii) $qV_b<E_x<q\phi$ (TFES): If the carriers have sufficient energy to over come the parabolic barriers in the depleted regions but not sufficient energy to over come the grain boundary barrier $q\phi$, then the potential barrier $qV(x)$ through which the carriers have to tunnel is given by

$$\left.\begin{aligned} qV(x) &= 0 && \text{for } |x| > W_{gb}/2 \\ qV(x) &= q\phi && \text{for } |x| < W_{gb}/2 \end{aligned}\right\} \quad (13)$$

In this case Thermionic field emission with scattering (TFES) from the grain boundary is possible.

(iii) $E_x > q\phi$ (TE): If the carriers are sufficiently energetic to over come the grain boundary barrier qϕ, then $qV(x) = 0$, $D(E_x) = 1$, and current transport is by the Thermionic emission over these barriers. So in this case thermionic emission (TE) is possible.

In general all the above conduction mechanisms occur in parallel. However, at a given temperature or with in a small range of temperature, carrier transport is dominated by one or two of these process. The present work is restricted to a practical range of temperatures and the following limitations have also been imposed while obtaining an analytical solution.

[i] The solution of current density is restricted to temperature at which the carriers have sufficient energy to over come the depletion region barriers tunnel through the much thinner grain- boundary barriers becomes more significant.

[ii] The average applied voltage per gain V_0 is much less than the height of the grain boundary barrier ($V_0 << q\phi$).

[iii] The maximum barrier height in the depletion region of the grains is much less than the height of the grain –boundary barrier ($V_b << q\phi$)

[iv] Complete ionization of the dopant atoms in the grains is assumed so that the carrier concentration in the neutral regions of the grains is equal to the dopant concentration there.

[v] The single –crystal energy band is applicable inside the crystallites.

[vi] One-dimensional majority –carrier transport is assumed, any contribution from the injection of minority carrier is neglected. The equivalent effective mass of single crystal silicon is used in the barrier.

At intermediate temperature only a few carrier have energies higher than the maximum height of the grain boundary barriers. Thus the contribution to current by Thermionic emission of carriers over the grain boundary barriers can be

neglected. Also the grain –boundary barrier are much thinner than the barriers in the depleted regions of the grains. Thus the probability of tunneling through the grain –boundary is higher than passing through depletion region & grain boundary barrier. Thus conduction is mainly controlled by carriers tunneling through the grain boundary barriers after being thermally emitted over the depletion region barriers; thus carriers whose value of E_x are in the range $qV_b < E_x < q\phi$. By including the above approximations equation (11) can be written in the form.

$$J = q\left(\frac{4\pi}{h^3}m_h^* kT\right)\left[\int_{qV_b+qV_{gb}/2}^{q\phi+qV_{gb}/2} \ln\left\{1+\exp\left[\frac{-\left(E_x+\xi-\frac{qV_{gb}}{2}-qV_L\right)}{kT}\right]\right\} D_{LR}(E_x)\,dE_x - \int_{qV_b-qV_{gb}/2}^{q\phi-qV_{gb}/2} \ln\left\{1+\exp\left[\frac{-\left(E_x+\xi+\frac{qV_{gb}}{2}+qV_R\right)}{kT}\right]\right\} D_{RL}(E_x)\,dE_x\right]$$

The above equation can further be simplified by considering only the carrier distributions $ln(1+X)\approx X$. so the equation become,

$$J = q\left(\frac{4\pi}{h^3}m_h^* kT\right)\left[\int_{qV_b+qV_{gb}/2}^{q\phi+qV_{gb}/2} \exp\left[\frac{-\left(E_x+\xi-\frac{qV_{gb}}{2}-qV_L\right)}{kT}\right] D_{LR}(E_x)\,dE_x - \int_{qV_b-qV_{gb}/2}^{q\phi-qV_{gb}/2} \exp\left[\frac{-\left(E_x+\xi+\frac{qV_{gb}}{2}+qV_R\right)}{kT}\right] D_{RL}(E_x)\,dE_x\right] \quad (15)$$

As current flow is predominantly due to carriers whose value of E_x are only slightly greater than the maximum height of the barriers in the depletion regions, thus the tunneling probability $D(E_x)$ can be simplified by expanding it using Taylor series around qV_b .(Appendix-D)

$\varepsilon_x = qV_b - E_x$

$$\therefore \ln D(E_x) = -[b_1 + c_1\varepsilon_x + f_1\varepsilon_x^2 + \ldots\ldots\ldots\ldots] \quad (16)$$

Where,

$$b_1 = \left\{ \frac{4\pi}{h} \int_a^b \left[2m_h^* (qV(x) - qV_b) \right]^{\frac{1}{2}} dx \right\}$$
$$c_1 = \left\{ \frac{2\pi}{h} \int_a^b \left[2m_h^* (qV(x) - qV_b) \right]^{\frac{-1}{2}} dx \right\} \quad (17)$$

For applied voltage much less than height of the grain boundary barrier $q\phi$ (assumption [ii] made earlier), b_1, c_1 and f_1 are independent of the applied voltage so that

$$D_{LR}(E_x) = D_{RL}(E_x) = D(E_x) \quad (18)$$

The constants b_1 and c_1 can be calculated by solving (17) using the appropriate barrier $qV(x)$. For carrier in the energy range $qV_b < E_x < q\phi$, the values of b_1, c_1 are given by (Appendix-E).

$$\left.\begin{aligned} b_1 &= \frac{4\pi}{h} W_{gb} \left(2m_h^*\right)^{1/2} (q\phi - qV_b)^{1/2} \\ c_1 &= \frac{2\pi}{h} W_{gb} \left(2m_h^*\right)^{1/2} (q\phi - qV_b)^{-1/2} \end{aligned}\right\} \quad (19)$$

The quadratic & higher order terms in the expansion of $D(E_x)$ can be neglected using assumption [iii] i.e. $qV_b << q\phi$, as they will contain the terms of $(q\phi - qV_b)^{\frac{-3}{2}}, (q\phi - qV_b)^{\frac{-5}{2}}$ etc. which become less & less as the negative power increases.

So the value of the $D(E_x)$ can be taken as follows;

$$D(E_x) = \exp[-(b_1 + c_1 \varepsilon_x)] \quad (20)$$

Using equation (20) in (15) the final expression of the current density given by;

$$J = q\left(\frac{4\pi}{h^3}m_h^* kT\right)\left[\int_{qV_b+qV_{gb}/2}^{q\phi+qV_{gb}/2}\left\{\exp\left[\frac{-\left(E_x+\xi-\frac{qV_{gb}}{2}-qV_L\right)}{kT}\right]\right\}\exp[-(b_1+c_1\varepsilon_x)]dE_x - \int_{qV_b-qV_{gb}/2}^{q\phi-qV_{gb}/2}\left\{\exp\left[\frac{-\left(E_x+\xi+\frac{qV_{gb}}{2}+qV_R\right)}{kT}\right]\right\}\exp[-(b_1+c_1\varepsilon_x)]dE_x\right] \quad (21)$$

After solving the integration (appendix-F) we get,

$$J = \frac{q}{(1-c_1kT)}\left(\frac{4\pi}{h^3}m_h^* k^2T^2\right)e^{-\xi/kT}e^{-(b_1+c_1qV_b)}\left[e^{\left(qV_L+\frac{c_1kTqV_{gb}}{2}\right)/kT}\left\{e^{-qV_b(1-c_1kT)/kT}-e^{-q\phi(1-c_1kT)/kT}\right\} - e^{-\left(qV_R+\frac{c_1kTqV_{gb}}{2}\right)/kT}\left\{e^{-qV_b(1-c_1kT)/kT}-e^{-q\phi(1-c_1kT)/kT}\right\}\right] \quad (22)$$

$$J = \frac{q}{(1-c_1kT)}\left(\frac{4\pi}{h^3}m_h^* k^2T^2\right)e^{-\xi/kT}e^{-(b_1+c_1qV_b)}\left\{e^{-qV_b(1-c_1kT)/kT}-e^{-q\phi(1-c_1kT)/kT}\right\}\left[e^{\left(qV_L+\frac{c_1kTqV_{gb}}{2}\right)/kT}-e^{-\left(qV_R+\frac{c_1kTqV_{gb}}{2}\right)/kT}\right] \quad (23)$$

Since according to our assumption $q\phi >> qV_b$ (for TFES)), thus ignoring terms of $q\phi$ in the exponential we get,

$$J = \frac{q}{(1-c_1kT)}\left(\frac{4\pi}{h^3}m_h^* k^2T^2\right)e^{-\xi/kT}e^{-(b_1+c_1qV_b)}\left\{e^{-qV_b(1-c_1kT)/kT}\right\}\left[e^{\left(qV_L+\frac{c_1kTqV_{gb}}{2}\right)/kT}-e^{-\left(qV_R+\frac{c_1kTqV_{gb}}{2}\right)/kT}\right] \quad (24)$$

Equation (24) shows that current density is a function of both the voltage drop across the grain boundary barrier and the voltage drops across the depleted regions on either side of grain boundary barrier. For the tunneling to be occurring the applied voltage V_0 should be much less than the height of the barrier in the depletion region ($V_0 << V_b$) under this condition voltage drop on left and right side is almost similar [4].

$$\therefore V_L = V_R = V_d$$

V_d is half of the voltage drop across the depletion region of the grains.
So the new from of (24) is,

$$J = \frac{q}{(1-c_1 kT)}\left(\frac{4\pi}{h^3} m_h^* k^2 T^2\right) e^{-\xi/kT}\, e^{-b_1}\, e^{-qV_b/kT}\, 2Sinh\left(\frac{qV_d + c_1 kTq\, V_{gb}/2}{kT}\right) \qquad (25)$$

Now the voltage drop across the grain boundary (V_{gb}) is given by (Appendix G) i.e.,

$$V_{gb} = \frac{W_{gb} N_G}{Q_t} 2V_d \qquad (26\ a)$$

Also

$$\therefore \quad V_0 = V_{gb} + 2V_d$$

$$V_0 = \left(\frac{W_{gb} N_G}{Q_t} 2V_d + 2V_d\right) \qquad (26\ b)$$

$$V_0 = 2V_d\left(\frac{W_{gb} N_G}{Q_t} + 1\right)$$

Using equation (26a) & (26b) in (25) we get;

$$J = \frac{2q}{(1-c_1 kT)}\left(\frac{4\pi}{h^3} m_h^* k^2 T^2\right) e^{-\xi/kT}\, e^{-b_1}\, e^{qV_b/kT}\, Sinh\left(\frac{1 + c_1 kTN_G\, W_{gb}/Q_t}{1 + \frac{N_G W_{gb}}{Q_t}} \cdot \frac{qV_o}{2kT}\right) \qquad (27)$$

This is the expression of the current density; It can be seen that the current density is dependent on the applied voltage, trapping density & barrier height of the grain region. Assuming that applied voltage V_o across the composite grain boundary is much less than kT, the assumption reduces equation (27) to

$$J = \frac{2q}{(1-c_1 kT)}\left(\frac{4\pi}{h^3} m_h^* k^2 T^2\right) e^{-\xi/kT}\, e^{-b_1}\, e^{-qV_b/kT}\left(\frac{1+c_1 kTN_G W_{gb}/Q_t}{1+\frac{N_G W_{gb}}{Q_t}} \cdot \frac{qV_o}{2kT}\right) \tag{28}$$

Now as we know that, $J = \sigma_{gb}\varepsilon_{gb} = \sigma_{gb}\dfrac{V_o}{L_{gb}}$

Therefore the conductivity of the composite grain boundary region σ_{gb} is given by

$$\sigma_{gb} = \frac{q^2 L_{gb}}{(1-c_1 kT)}\left(\frac{4\pi}{h^3} m_h^* kT\right) e^{-\xi/kT}\, e^{-b_1}\, e^{-qV_b/kT}\left(\frac{1+c_1 kTN_G W_{gb}/Q_t}{1+\frac{N_G W_{gb}}{Q_t}}\right) \tag{29}$$

where $L_{gb} = 2W + W_{gb}$ is the length of the composite grain boundary region.

The average resistivity can be obtained as follows; in general the voltage drop across a single crystal V_a is divided between the composite grain-boundary region (the grain boundary and the adjacent region in the grains) and the grain itself.

$$V_a = V_o + V_g$$

Where V_g is the voltage drop across the undepleted grain.

$$\rho = \frac{V_a}{JL} = \frac{V_g}{JL} + \frac{V_o}{JL} = \frac{L_g V_g}{LJL_g} + \frac{L_{gb}}{L}\cdot\frac{V_o}{JL_{gb}} \tag{30}$$

$$\rho = \frac{L_g}{L}\cdot\rho_g + \frac{L_{gb}}{L}\cdot\rho_{gb}$$

3.3 Calculation of Resistivity & Mobility for Various Doping Conditions

Current density or the conductivity expression was derived under the assumption listed before but with out any limitation on the dopant concentration. However, the width of depleted regions in the grains due to carrier trapping is a function of the dopant concentration. Therefore, the dopant concentration indirectly affects the conditions under which the above theory is applicable.

3.3.1 At High Dopant Concentration

From equation (29) we have

$$\sigma_{gb} = \frac{q^2 L_{gb}}{(1-c_1 kT)} \left(\frac{4\pi}{h^3} m_h^* kT\right) e^{-\xi/kT} e^{-b_1} e^{-qV_b/kT} \left(\frac{1+c_1 kT N_G W_{gb}/Q_t}{1+\frac{N_G W_{gb}}{Q_t}} \right) \qquad (29)$$

Assuming the complete ionization of the dopant atoms within the grain the carrier concentration in the grain is given by.

$$n = N_v \exp\left(\frac{-\xi}{kT}\right) = 2\left(\frac{2\pi m_h^* kT}{h^2}\right)^{3/2} \exp\left(\frac{-\xi}{kT}\right) \approx N_G \qquad (31)$$

With this condition equation (29) becomes as follows

$$\sigma_{gb} = \frac{q^2 L_{gb} N_G}{(1-c_1 kT)} \left(\frac{1}{2\pi m_h^* kT}\right)^{1/2} e^{-b_1} e^{-qV_b/kT} \left(\frac{\frac{Q_t}{N_G W_{gb}} + c_1 kT}{1+\frac{Q_t}{N_G W_{gb}}} \right) \qquad (32a)$$

And,

$$J_{TFES} = \frac{q^2 N_G}{(1-c_1 kT)} \left(\frac{1}{2\pi m_h^* kT}\right)^{1/2} e^{-b_1} e^{-qV_b/kT} \left(\frac{\frac{Q_t}{N_G W_{gb}} + c_1 kT}{1+\frac{Q_t}{N_G W_{gb}}}\right) V_o \qquad (32b)$$

Equation (32a) is the conductivity equation for highly B-doped polysilicon, which depends on grain boundary width and depletion potential barrier. It is a transcendental equation for W_{gb}; in the next chapter calculation of W_{gb} is done numerically using some experimental values and fitting parameter. So starting with equation (19), values of constants b_1 & c_1 depend on three parameter $W_{gb}, q\phi$ and qV_b. In the present work we have calculated the W_{gb} using the experimental values of $q\phi$ and qV_b so for a particular sample $q\phi$ and qV_b will be constant. Thus b_1 and c_1 are taken as function of W_{gb} as follows.

$$b_1 = bW_{gb} \;\&\; c_1 = cW_{gb} \qquad (33a)$$

Where

$$\left.\begin{aligned} b &= \frac{4\pi}{h}\left(2m_h^*\right)^{1/2}\left(q\phi - qV_b\right)^{1/2} \\ c &= \frac{2\pi}{h}\left(2m_h^*\right)^{1/2}\left(q\phi - qV_b\right)^{-1/2} \end{aligned}\right\} \qquad (33b)$$

Also define

$$a = q^2 N_G \left(\frac{1}{2\pi m_h^* kT}\right)^{1/2} e^{-qV_b/kT}$$

Using equation (33a) in equation (33b) we get,

$$\sigma_{gb} = \frac{aL_{gb} e^{-bW_{gb}}}{\left(1-cW_{gb}kT\right)} \frac{\left(\frac{Q_t}{N_G W_{gb}} + ckTW_{gb}\right)}{\left(1+\frac{Q_t}{N_G W_{gb}}\right)} \qquad (34)$$

3.3.2 Low Dopant Concentration

At low dopant concentration the height of the depletion region barrier qV_b has a maximum value approximately $E_g/2$, where E_g is the band gap of the single crystal silicon (1.1eV). Height of the grain boundary barrier $q\phi_{gb}= E_{gb}/2$ is expected to be of the order of 0.6 –0.8 eV (Section IV, i). Thus at low dopant concentration, qV_b may be comparable to $q\phi$.

So for low dopant concentration $q\phi \approx qV_b$ thus the assumption [iii] has been violated and hence [i]. It must be noted that assumptions [iii] & [i] have been used in many places to derive equation (29). Since depletion barrier height is comparable to grain boundary barrier, the tunneling probability becomes one & thermionic emission (TE) will be dominant over thermionic emission field emission with scattering (TFES). Therefore, at low dopant concentration, conduction properties can be calculated by thermionic emission (TE) and we cannot calculate the properties using thermionic field emission with scattering (TFES).

3.3.3 Thermionic Emission (TE)

As mentioned above, at low doping concentration the depletion barrier is comparable to potential barrier across the grain boundary. Hence tunneling probability is unity. Therefore thermionic emission becomes dominant. To calculate current density due to TE we simply put 1 for tunneling probability in equation (15). Hence

$$D(E_x) = exp[-(b_1 + c_1\varepsilon_x)]=1 \quad or\ b_1,c_1= 0 \tag{35}$$

Hence in equation (25) given below,

$$J = \frac{q}{(1-c_1kT)}\left(\frac{4\pi}{h^3}m_h^*k^2T^2\right)e^{-\xi/kT}\ e^{-b_1}\ e^{-qV_b/kT}\ 2Sinh\left(\frac{qV_d+c_1kTq^{V_{gb}/2}}{kT}\right) \tag{25}$$

After putting $b_1 = 0$ & $c_1 = 0$ equation (25) becomes,

$$J = q\left(\frac{4\pi}{h^3}m_h^* k^2 T^2\right) e^{-\xi/kT}\, e^{-b_1}\, e^{-qV_b/kT}\, 2Sinh\left(\frac{qV_d}{kT}\right) \tag{36}$$

$\because V_0 << kT$ Consequently $V_d << kT$ and assuming the complete ionization of the dopant atoms within the grain the carrier concentration in the grain is given by.

$$n = N_v \exp\left(\frac{-\xi}{kT}\right) = 2\left(\frac{2\pi m_h^* kT}{h^2}\right)^{3/2} \exp\left(\frac{-\xi}{kT}\right) \approx N_G$$

With these values equation (36) gives the thermionic current density as,

$$J_{TE} = q^2 N_G \left(\frac{1}{2\pi m_h^* kT}\right)^{1/2} e^{-qV_b/kT}\, 2V_d$$

Using the relation of equation (26b)

$$J_{TE} = q^2 N_G \left(\frac{1}{2\pi m_h^* kT}\right)^{1/2} e^{-qV_b/kT} \frac{V_o}{\left(\frac{W_{gb}N_G}{Q_t}+1\right)} \tag{37}$$

The conductivity is given by,

$$\therefore \sigma_{TE} = \frac{q^2 L N_G}{\left(\frac{W_{gb}N_G}{Q_t}+1\right)} \left(\frac{1}{2\pi m_h^* kT}\right)^{1/2} e^{-qV_b/kT} \tag{38a}$$

Hence

$$\therefore \rho_{TE} = \frac{\left(\frac{W_{gb}N_G}{Q_t}+1\right)}{q^2 L N_G} \left(2\pi m_h^* kT\right)^{1/2} e^{qV_b/kT} \tag{38b}$$

And

$$\mu_{TE} = \frac{qL}{\left(\frac{W_{gb}N_G}{Q_t}+1\right)}\left(\frac{1}{2\pi m_h^* kT}\right)^{1/2} e^{-qV_b/kT} \tag{38c}$$

This is the conductivity equation due to thermionic emission. We can further simplify this equation, by assigning $\frac{W_{gb}N_G}{Q_t} << 1$

$$\therefore \sigma_{TE} = q^2 LN_G\left(\frac{1}{2\pi m_h^* kT}\right)^{1/2} e^{-qV_b/kT} \tag{38d}$$

This equation is same as obtained by Seto [2], Lu [7], Baccarani [3], though they neglect the grain boundary effect completely, equation (38d) better explain the experimental results at low doping concentration.

Equation (38c) is the mobility equation at low doping concentration. We will see in chapter 4 that it will show the deviation from the experimental values at high dopant concentration. In the following derivation we have shown that polysilicon mobility reaches to single crystal range at high dopant concentration. We have equation (37),

$$J_{TE} = q^2 N_G\left(\frac{1}{2\pi m_h^* kT}\right)^{1/2} e^{-qV_b/kT} \frac{V_o}{\left(\frac{W_{gb}N_G}{Q_t}+1\right)}$$

Say $G = \left(\frac{WgbN_G}{Q_t}+1\right)$

$$\therefore J_{TE} = q^2 N_G\left(\frac{1}{2\pi m_h^* kT}\right)^{1/2} e^{-qV_b/kT} V_o G \tag{37a}$$

Current density due to undepleted region.

$$J_G = \sigma_G E_G = qN_G \mu_{mono} \frac{V_g}{(L-2W)} \tag{37b}$$

where μ_{mono} is the mobility of single crystal.

Current density must be maintained at any point of the sample, therefore equating equations (37a) and (37b).

$J_G = J_{TE}$

$$qN_G \mu_{mono} \frac{V_g}{(L-2W)} = q^2 N_G \left(\frac{1}{2\pi m_h^* kT}\right)^{1/2} e^{-qV_b/kT} V_o G$$

If V_a is the applied voltage $V_a=V_o+V_g$, Eliminating V_o we get,

$$V_g = \frac{\frac{qG}{(2\pi m_h^* kT)^{1/2}} e^{-qV_b/kT} V_a}{\left[\frac{\mu_{mono}}{(L-2W)} + \frac{qG}{(2\pi m_h^* kT)^{1/2}} e^{-qV_b/kT}\right]}$$

Final expression of current density from equation (37b) is given by using this potential across the grain (V_g),

$$J_G = \frac{qN_G \frac{\mu_{mono}}{(L-2W)} \frac{qG}{(2\pi m_h^* kT)^{1/2}} e^{-qV_b/kT} V_a}{\left[\frac{\mu_{mono}}{(L-2W)} + \frac{qG}{(2\pi m_h^* kT)^{1/2}} e^{-qV_b/kT}\right]}$$

Or

$$\left(\frac{J_G}{qN_G}\right) = \frac{V_a}{\left[\frac{(L-2W)}{\mu_{mono}} + \frac{(2\pi m_h^* kT)^{1/2}}{qG} e^{qV_b/kT}\right]}$$

Dividing both sides by L and rearranging the equation.

$$\left(\frac{qN_G}{J_G}\right)\left(\frac{V_a}{L}\right)=\left[\frac{(L-2W)}{\mu_{mono}L}+\frac{(2\pi m_h^* kT)^{1/2}}{qLG}e^{qV_b/kT}\right]$$

If E_{ext} is the external applied field and V_d is the drift velocity of a hole. Using equation (38c) we get,

$$\left(\frac{E_{ext}}{V_d}\right)=\left[\frac{1}{\mu_{mono}}.\frac{(L-2W)}{L}+\frac{1}{\mu_{TE}}\right]$$

or

$$\frac{1}{\mu_{eff}}=\left[\frac{1}{\mu_{mono}}.\frac{(L-2W)}{L}+\frac{1}{\mu_{TE}}\right]$$

At high dopant concentration $2W << L$

$$\frac{1}{\mu_{eff}}\approx\left[\frac{1}{\mu_{mono}}+\frac{1}{\mu_{TE}}\right] \text{ Or } \mu_{eff}=\frac{\mu_{mono}\mu_{TE}}{(\mu_{mono}+\mu_{TE})} \tag{39}$$

This equation show how effective mobility related with singe crystal and thermionic mobility.. In chapter 4 plot is shown which show the difference of μ_{eff} , μ_{TE} and the experimental values at high dopant concentration.

3.3.4 Combined Effect of TFES & TE

While deriving thermionic emission we have neglected the effect of scattering or tunneling through the barrier, though we cannot neglect the tunneling effect completely there is always some probability for the tunneling so their combined mechanism should be considered. Considering both TFES and TE effects the current density from equations (32b) and (37) is given by,

$$J_{Total} = J_{TFES} + J_{TE} \tag{40}$$

$$J = q^2 N_G \left(\frac{1}{2\pi m_h^* kT}\right)^{1/2} V_o\,(TFES + TE) \tag{40a}$$

Now the final expression of the resistivity is given by equation (30)

$$\begin{aligned} \rho &= \frac{L_g}{L}\cdot\rho_g + \frac{L_{gb}}{L}\cdot\rho_{gb} \\ \rho &= \frac{L_{gb}}{L}\cdot\rho_{gb} + \rho_g\left(1 - \frac{2W}{L} - \frac{W_{gb}}{L}\right) \end{aligned} \tag{30}$$

Using the relation $J = \dfrac{V_o}{\rho_{gb} L_{gb}}$ and equation (40a) in equation (30) we get,

$$\rho = \frac{(2\pi m_h^* kT)^{1/2}}{q^2 L N_G}\left(\frac{1}{TFES + TE}\right) + \rho_g\left(1 - \frac{2W}{L} - \frac{W_{gb}}{L}\right) \tag{41}$$

This is the average resistivity equation of the polysilicon. Using this equation calculation of resistivity at low and high dopant concentration is done.

3.3.4.1 At High Dopant Concentration

At high dopant concentration only TFES is effective and the contribution by thermionic emission is negligible, so average resistivity is given by thermionic field emission with scattering (TFES) only. So putting equation (34) in (30) we get the average resistivity at high doping concentration.

$$\rho = \frac{(2\pi m_h^* kT)^{1/2}}{q^2 L N_G} \frac{(1 - cW_{gb}kT)\left(1 + \dfrac{Q_t}{N_G W_{gb}}\right)}{\left(\dfrac{Q_t}{N_G W_{gb}} + ckTW_{gb}\right)} e^{bW_{gb}} e^{qV_b/kT} + \left(1 - \frac{2W}{L} - \frac{W_{gb}}{L}\right)\rho_G \tag{42a}$$

If we also consider the TE with TFES the equation changes to,

$$\rho = \frac{(2\pi m_h^* kT)^{1/2}}{q^2 L N_G} e^{qV_b/kT} \frac{1}{\left[\frac{\left(\frac{Q_t}{N_G W_{gb}} + ckTW_{gb}\right) e^{-bW_{gb}}}{(1 - cW_{gb} kT)\left(1 + \frac{Q_t}{W_{gb} N_G}\right)} + \frac{1}{\left(\frac{N_G W_{gb}}{Q_t} + 1\right)}\right]} + \left(1 - \frac{2W}{L} - \frac{W_{gb}}{L}\right)\rho_G \qquad (42b)$$

And $$\mu = \frac{1}{qN_G\rho} \qquad (42c)$$

This is the resistivity equation at high dopant concentration, which depends on grain boundary width, grain size, trapping density, potential barrier, temperature and resistivity of the crystallites. Equation (42b) is used for the numerical calculation of grain boundary width using experimental results in the next chapter.

3.3.4.2 At Low Dopant Concentration

Contribution to the current density by both TFES and TE at low doping concentration is the sum of both the currents in the grain

$$J_{Total} = J_{TFED} + J_{TE}$$

As explained in section 3.3.2 at low doping concentration thermionic emission is the dominant phenomenon, so current density due to thermionic field emission with scattering (J_{TFED}) can be neglected.

$\therefore$

$$J_{Total} = J_{TE}$$

$$J_{Total} = q^2 N_G \left(\frac{1}{2\pi m_h^* kT}\right)^{1/2} e^{-qV_b/kT} V_O \quad (43a)$$

$$\therefore \sigma_{eff} = q^2 N_G L \left(\frac{1}{2\pi m_h^* kT}\right)^{1/2} e^{-qV_b/kT} \quad (43b)$$

$$\mu_{eff} = q L \left(\frac{1}{2\pi m_h^* kT}\right)^{1/2} e^{-qV_b/kT} \quad (43c)$$

Using Equation (43b) effective resistivity can be calculated at low dopant concentration.

$$\rho = \frac{\left(2\pi m_h^* kT\right)^{1/2}}{q^2 N_G L} e^{qV_b/kT} \quad (43d)$$

In the present work special interest is shown to calculate average carrier concentration at low doping concentration, to calculate average carrier concentration we have used the following equation.

$$N_G = \frac{1}{q\rho\mu} \quad (43e)$$

These equations (43a-d) are used to calculate current density, mobility & resistivity for various low doping conditions and the results are compared with experimental values in the next chapter.

Chapter 4

Numerical Calculations And Results

4.1.1 Numerical Calculation of W_{gb}

In chapter 3 derivation of resistivity is done analytically (equation 42). In the present section numerical calculation of grain boundary width is done. The experimental data have been used to numerically calculate W_{gb}. To solve equation (42) numerically we need the depletion width, which can be calculated using the following formula for single crystal silicon [10] using the diode approximation between depletion width and grain boundary (assumption [v]).

$$W = \sqrt{\frac{2\varepsilon V_b}{qN_G\left(1+\frac{N_G}{N_t}\right)}} \tag{44a}$$

where N_G &N_t are the charge densities within grain and grain boundary. Charge density inside the grain boundary is given by carriers trapped inside the grain boundary, i.e. N_t

Now the two cases arise for the depletion width.

(i) Depletion width at very high dopant concentration

(ii) Depletion width at moderate dopant concentration

In case (i), at high dopant concentration depletion barrier height is extremely low. Under this case $V_b = 0$ and consequently W≈0 from equation (44a). With these values in equation (42a) gets modified as follows.

$$\rho = \frac{\left(2\pi m_h^* kT\right)^{1/2}}{q^2 L N_G} \frac{\left(1-cW_{gb}kT\right)\left(1+\frac{Q_t}{W_{gb}N_G}\right)}{\left(\frac{Q_t}{N_G W_{gb}}+ckTW_{gb}\right)} e^{bW_{gb}} e^{qV_b/kT} + \left(1-\frac{2W}{L}-\frac{W_{gb}}{L}\right)\rho_G$$

$$\rho = \frac{(2\pi m_h^* kT)^{1/2}}{q^2 L N_G} \frac{\left(1-cW_{gb}kT\right)\left(1+\frac{Q_t}{W_{gb}N_G}\right)}{\left(\frac{Q_t}{N_G W_{gb}}+ckTW_{gb}\right)} e^{bW_{gb}} e^{qV_b/kT} + \left(1-\frac{W_{gb}}{L}\right)\rho_G \qquad (45)$$

Equation of average resistivity only due to thermionic field emission with scattering from the barrier (TFES) is taken for the grain boundary width calculation (W_{gb}) as at high dopant concentration TFES is a dominant phenomenon, so we had neglected contribution due to TE. To solve equation (45) we need the following experimental data.

S.No.	Data Taken from Experiments	
	Physical parameter	Value
1.	Q_t	$3.34\times10^{12}\,cm^{-2}$
2.	N_G	$2.6\times10^{19}\,cm^{-3}$
3.	ρ	$4.2x10^{-3}\,\Omega.cm$
4.	ρ_G	$5.18\times10^{-3}\,\Omega.cm$
5.	qϕ	$.66eV$
6.	L	$200A^0$
7.	T	$27\ ^0C$
8.	ε	$1.0433x10^{-10}$
9.	m_h^*	$.23m_0 = 2.093\times10^{-31}$
10.	μ_{h_g}	$480cm^2V^{-1}\sec^{-1}$
11.	K	$1.38\times10^{19}\,kg.cm^2.sce^{-2}K^{-1}$

Table 1: The Experimental data from [2,4 & 7] for very high doping

Calculated value of *b* & *c* using equations (33b) and values given in the Table above

1.	b	$3.9910 \times 10^{7}\ cm^{-1}$
2.	c	$1.8897 \times 10^{22}\ kg^{-1} cm^{-3}\ \sec^2$

Table 2: Constants calculated

Using the tabulated values, transcendental equation (45) can be solved numerically. The Newton-Raphson iteration method (Appendix-H) in the Mat Lab application software was used [34] to calculate W_{gb}. W_{gb} of ~ $11.86A^{\circ}$ was obtained for high doping.

Now in case (ii) when the doping is moderate, barrier height and depletion width are not negligible, so these have also been calculated.

$$W = \sqrt{\frac{2\varepsilon V_b}{qN_G\left(1+\frac{N_G}{N_t}\right)}} \tag{44a}$$

Or

$$W = \sqrt{\frac{2\varepsilon V_b}{qN_G\left(1+\frac{N_G W_{gb}}{Q_t}\right)}} \tag{44b}$$

and equation (42a)

$$\rho = \frac{\left(2\pi m_h^* kT\right)^{1/2}}{q^2 L N_G} \frac{\left(1-cW_{gb}kT\right)\left(1+\frac{Q_t}{W_{gb}N_G}\right)}{\left(\frac{Q_t}{N_G W_{gb}}+ckTW_{gb}\right)} e^{bW_{gb}} e^{qV_b/kT} + \left(1-\frac{2W}{L}-\frac{W_{gb}}{L}\right)\rho_G \tag{42a}$$

Equation (42a) is a transcendental equation, using equation (44b) and following the similar procedure mentioned above with the following experimental values given in the Table 3 and 4.

S.No.	Data Taken from Experiments	
	Physical parameter	Value
1.	Q_t	$3.34\times10^{12}cm^{-2}$
2.	N_G	$5\times10^{18}cm^{-3}$
3.	qV_b	$0.0335eV$
4.	ρ	$0.85\Omega.cm$
5.	ρ_G	$0.02\Omega.cm$
6.	$q\phi$	$.66eV$
7.	L	$200A^0$
8.	T	$27\ ^0C$
9.	ε	$1.0433\text{x}10^{-10}$
10.	m_h^*	$.23m_0 = 2.093\times10^{-31}$
11.	μ_{h_g}	$60cm^2V^{-1}\sec^{-1}$
12.	K	$1.38\times10^{19}kg.cm^2.sce^{-2}K^{-1}$

Table 3: The Experimental data from [2,4& 7] for very high doping

Calculated value of *b, c* using equations (33b) and values given in the Table above.

1.	*B*	$3.8884\text{x}10^7cm^{-1}$
2.	*C*	$1.9395\times10^{22}kg^{-1}cm^{-3}sce^2$

Table 4: Constants calculated

Using these values in equation (42a) W_{gb} comes out to be $\approx 11.89A^0$.It can be seen that change in the value of grain boundary width is negligible with the change in dopant concentration. So grain boundary width is not a function of dopant concentration. Similar calculation was done for grain size $L=1220A^0$ and the trapping density $Q_t= 1.9x10^{12}cm^{-2}$ at room temperature the grain boundary

width comes out to be $27.35A^0$ for very high doping and $27.87A^o$ for moderately high doping concentration.

4.1.2 Resistivity at High Doping Concentration

Resistivity at high doping concentration is governed by equation (42),

$$\rho = \frac{(2\pi m_h^* kT)^{1/2}}{q^2 L N_G} e^{qV_b/kT} \left[\frac{1}{\left(\frac{Q_t}{N_G W_{gb}} + ckTW_{gb} \right) e^{-bW_{gb}} + \frac{1}{\left(\frac{N_G W_{gb}}{Q_t} + 1 \right)}} \right] + \left(1 - \frac{2W}{L} - \frac{W_{gb}}{L} \right) \rho_G$$

$\rho_{(TFES+TE)}$ ρ_g

If we put the numerical values in the equation, we find that at high doping concentration, resistivity is of the range of single crystal as shown in Table 5, and the first term in the above equation makes negligible contribution to resistivity. Thus at high doping concentration resistivity of grain becomes dominant.

S.No.	L=200A°			
	Doping Concentration (cm^{-3})	Experimental Resistivity $[\Omega.cm]$	Resistivity of Composite G.B Region $\rho_{(TFES+TE)}$ $[\Omega.cm]$	Resistivity of non depleted Grain ρ_g $[\Omega.cm]$
1.	$5x10^{18}$	0.85	$7.4829x10^{-4}$	.846
2.	$1x10^{19}$	.00278	$1.900x10^{-4}$	.00238
3.	$5x10^{19}$	$4.2x10^{-3}$	$3.35x10^{-5}$	$4.13x10^{-3}$

Table 5: Comparisons Between Resistivities

4.2 Theoretically Calculated Values & Various Plots

Using equations derived in the previous chapter along with the parameters of the Tables 1-4 the different electrical parameters average carrier concentration, barrier height, mobility, resistivity and current density are calculated and presented in the respective Tables at room temperature. In the present work our special interest is to calculate average carrier concentration at low doping concentration. We have used equation (43e) to calculate average carrier concentration. Therefore we need mobility and resistivity, hence barrier height. A brief procedure how these parameters are calculated is shown below.

(i) Barrier height given in Table 6a is calculated using equations from section 2.2.3. Values of Q_t, L, q and ε are given in Table 1. Trapping density $1.9\text{x}10^{12}\text{cm}^{-2}$ is taken for L=1220$A^o$from[7,20]. After calculating barrier height for different doping concentration and grain size, Average mobility shown in Table 6a was calculated using the empirical equation (43f) from section 4.2.1 and using the data of Table 1. Different mobility μ_{mono}, μ_{TE} and μ_{eff} shown in Table 6b. μ_{mono} is taken from [21] and μ_{TE}, μ_{eff} are calculated using equations (38c) and (39) respectively.

(ii) Table (7-8) shows the mobility variation considering contribution from TE, TFES, and TFES+TE along with experimental values at two different grain size L=200 A^o and L=1220A^o respectively. Equations (38c & 39), (42c & 42a) and (42c & 42b) are used for mobility calculation due to TE, TFES and TFES+TE respectively. Experimental values of Mobilities for the comparison are taken from [2] and [20,21,24] for L=200 A^o and L=1220 A^o respectively.

(iii) Table 9 shows the mobility values as a function of $1/kT$. All values were calculated using equation (43f) from section 4.2.1 for grain size 1220A^o and barrier potential 0.078eV[20].

(iv) Average carrier concentration shown in Table 10 is calculated using equation (43e). Resistivity values are taken from [2,7,20] for L=200A°

and from [7,20] for L=1220A° the calculated average mobility values shown in Table 6a are used for the calculation.

(v) Table (11-13) shows the resistivity variation considering contribution from TE, TFES and TFES+TE along with experimental values at two different grains size L=200A^o and L=1220 A^o respectively. Equations (38b), (42a) and (42b) are used for the resistivity calculation due to TE, TFES and TFES+TE respectively. Experimental values of resistivity are taken from [2,7,20] for L=200A^o and from [7,20] for L=1220A^o.

(vi) Table 14 shows the resistivity values at different grain size. Values are calculated using equation (43d) at doping concentration N=1x$10^{17}$$cm^{-3}$ and trapping density 4.4x$10^{12}$$cm^{-2}$[32].

(vii) Table 15 shows the current density at different operating voltages. These values were calculated using equation (43a), other experimental data needed are taken from [2], [22].

4.2.1 Plots and Corresponding Data of "Barrier Height Vs Doping Concentration" and "Mobility Vs Doping Concentration"

Plot of mobility Vs doping concentration is drawn using equation (43c), to match calculated values with experimental results two additional fitting parameters f and n are introduced here. These fitting parameters cannot be attributed to theoretical inaccuracy; it is due to two possible reasons. One is that the effective Richardson constant (effective hole mass) is much smaller than in single crystal, which may occur in such a disordered structures as polysilicon. The second is that some transmission probability exists when carriers pass through the complicated grain boundary by either scattering or recombination.

So equation (43c) with these fitting parameters is given by,

$$\mu = fqL\left(\frac{1}{2\pi m_h^* kT}\right)^{1/2} e^{-qV_b/nkT} \qquad (43f)$$

f is a scale factor which modifies the effective Richardson,S constant of a single crystal when used in such a highly disordered structure. Now equation (43f) becomes an empirical equation analogous to resistivity equation in [7,20,21]. In Table 6, mobility calculated from empirical equation (43f) is shown and compared with the experimental mobility values [7,20] in the following sections.

Values of the fitting parameters from [7] are given below,

f=0.12 , n= 6.49 for L=200A^o

f=0.060, n=1.22 for L=1220A^o

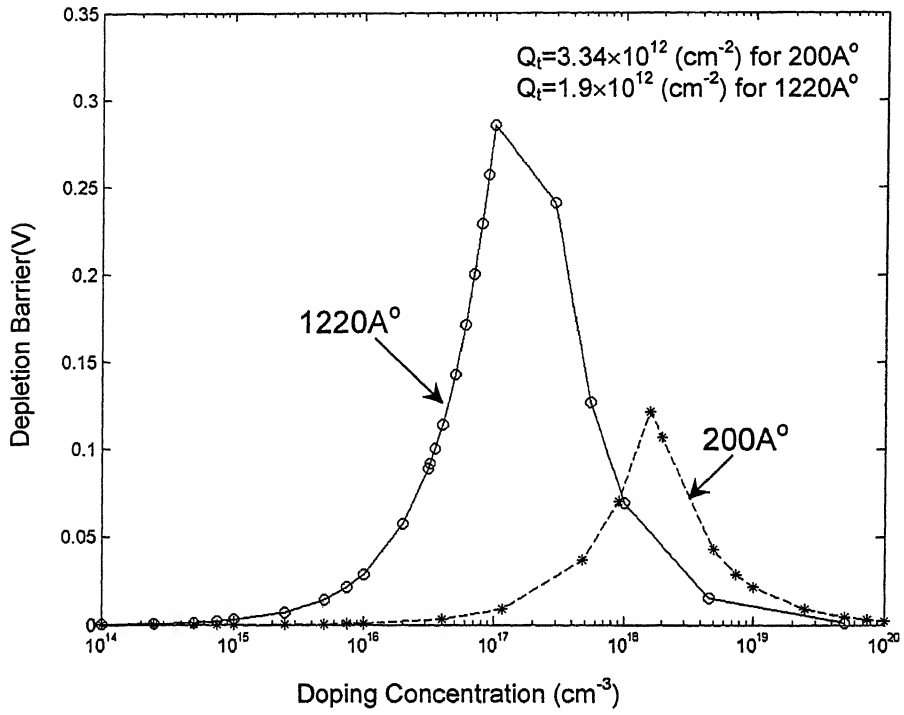

Figure 7: Doping concentration Vs Barrier height at room temperature

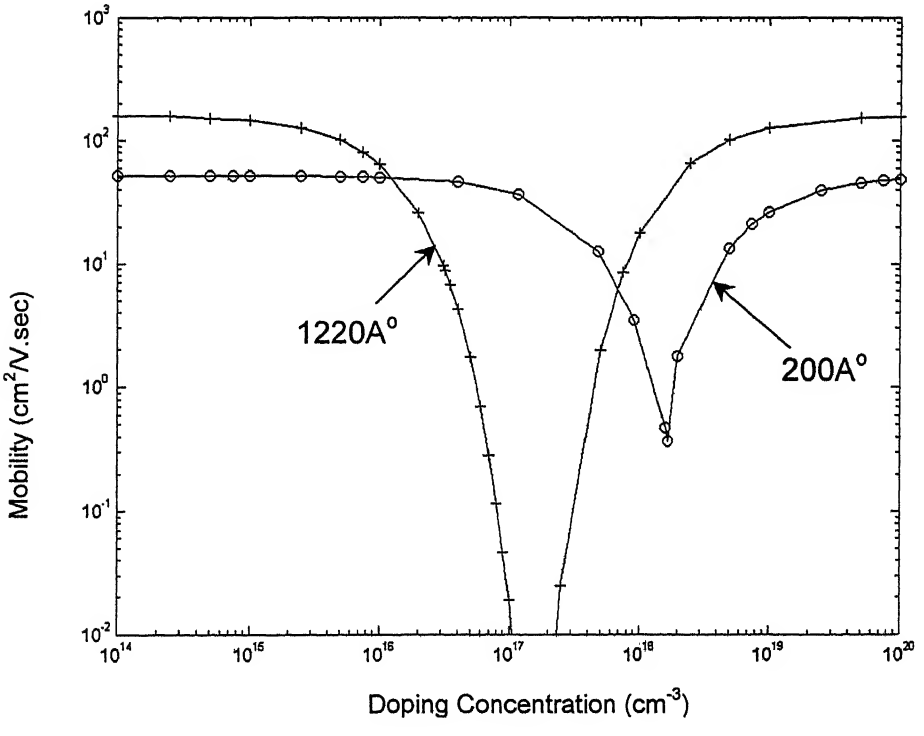

Figure 8a: Plot doping concentration Vs Mobility for grain size 200A° and 1220A°

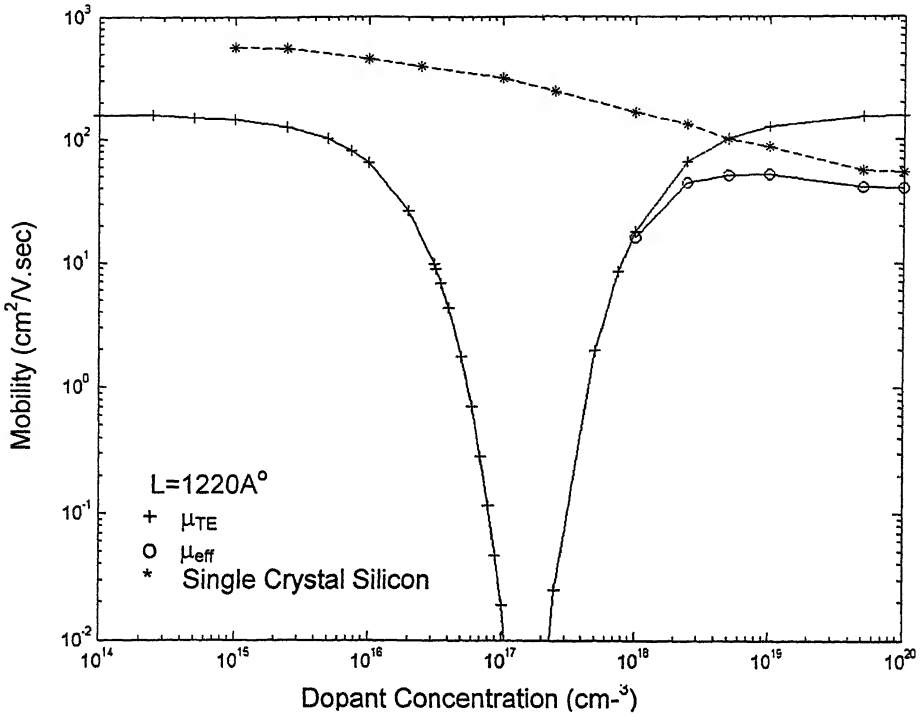

Figure 8b: Plot doping concentration Vs effective TE and single crystal mobility

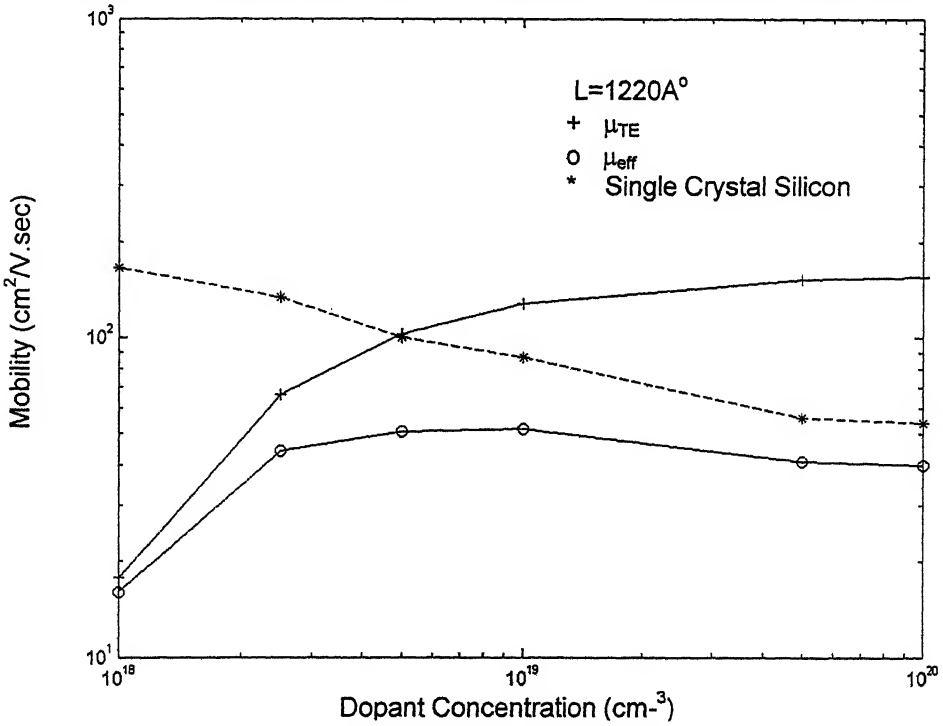

Figure 8c: Plot at high doping concentration Vs effective, TE, and single crystal mobility

S.No.	Grain Size=1220 A^{o}			Grain Size=200 A^{o}		
	Doping Concentration (cm^{-3})	Barrier Height (V)	Average Mobility ($cm^2/V.sec$)	Doping Concentration (cm^{-3})	Barrier Height (V)	Average Mobility ($cm^2/V.sec$)
1.	1.0×10^{14}	0.0003	157.3008	1.0×10^{14}	7.66×10^{-6}	52.0269
2.	2.5×10^{14}	0.0007	158.7290	2.5×10^{14}	1.91×10^{-5}	52.0038
3.	5.0×10^{14}	0.0014	151.7153	5.0×10^{14}	3.83×10^{-5}	51.9652
4.	7.5×10^{14}	0.002	149.6323	7.5×10^{14}	5.7×10^{-5}	52.0423
5.	1.0×10^{15}	0.0029	145.0114	1.0×10^{15}	7.66×10^{-5}	51.8883
6.	2.5×10^{15}	0.0071	126.6255	2.5×10^{15}	1.91×10^{-4}	51.6582
7.	5.0×10^{15}	0.0143	101.0150	5.0×10^{15}	3.83×10^{-4}	51.2769
8.	7.5×10^{15}	0.0214	80.5844	7.5×10^{15}	0.0006	50.8984
9.	1.0×10^{16}	0.0285	64.2859	1.0×10^{16}	0.0008	50.5227
10.	2.0×10^{16}	0.0571	26.0361	3.9811×10^{16}	0.0031	46.2508
11.	3.1×10^{16}	0.0885	9.6334	1.1749×10^{17}	0.0090	36.7405
12.	3.2×10^{16}	0.0913	8.8009	4.7863×10^{17}	0.0367	12.5994
13.	3.5×10^{16}	0.0999	6.7106	9.1201×10^{17}	0.0699	3.4881
14.	4.0×10^{16}	0.1141	4.2707	1.5849×10^{18}	0.1215	0.4749
15.	5.0×10^{16}	0.1427	1.7296	1.67×10^{18}	0.1281	0.3690
16.	6.0×10^{16}	0.1712	0.7005	2.0×10^{18}	0.1069	1.7592
17.	7.0×10^{16}	0.1997	0.2837	5.0×10^{18}	0.0428	13.4257
18.	8.0×10^{16}	0.2283	0.1149	7.5×10^{18}	0.0285	21.0900
19.	9.0×10^{16}	0.2568	0.0465	1.0×10^{19}	0.0214	26.4330
20.	1.0×10^{17}	0.2853	0.0188	2.5×10^{19}	0.0086	39.6892
21.	1.55×10^{17}	0.4423	0.0001	5.0×10^{19}	0.0043	45.4480
22.	2.88×10^{17}	0.2403	0.0247	7.5×10^{19}	0.0029	47.5476
23.	5.46×10^{17}	0.1267	1.9793	1.0×10^{20}	0.0021	48.6335
24.	1.0×10^{18}	0.0692	66.0428			
25.	4.64×10^{18}	0.0149	102.3861			
26.	5.0×10^{19}	0.0014	151.9199			
27.	1.0×10^{20}		155.2872			

Table 6 a:Doping Concentration, Barrier Height and Mobility

S.No.	Doping Concentration (cm^{-3})	μ_{mono} ($cm^2/V.sec$)[21]	μ_{TE} ($cm^2/V.sec$)	μ_{eff} ($cm^2/V.sec$)
	1.0×10^{15}	562.34		
	2.5×10^{15}	554.30		
	1.0×10^{16}	453.15		
	2.5×10^{16}	392.41		
	1.0×10^{17}	365.17		
	2.5×10^{17}	294.27		
	1.0×10^{18}	165.48	17.720	16.0099
	2.5×10^{18}	133.35	66.040	44.1685
	5.0×10^{18}	100.00	102.38	50.5895
	7.5×10^{18}	93.05		
	1.0×10^{19}	86.59	127.48	51.5675
	2.5×10^{19}	64.93		
	5.0×10^{19}	56.23	151.91	41.0421
	7.5×10^{19}	54.63		
	1.0×10^{20}	53.85	155.28	39.9887

Table 6 b: Doping Concentration, Barrier Height and Mobility

4.2.2 Plots and Corresponding Data of "Mobility Vs Doping Concentration" For TFES+TE, TFES, TE and Experimental Values (200 A°Grain Size)

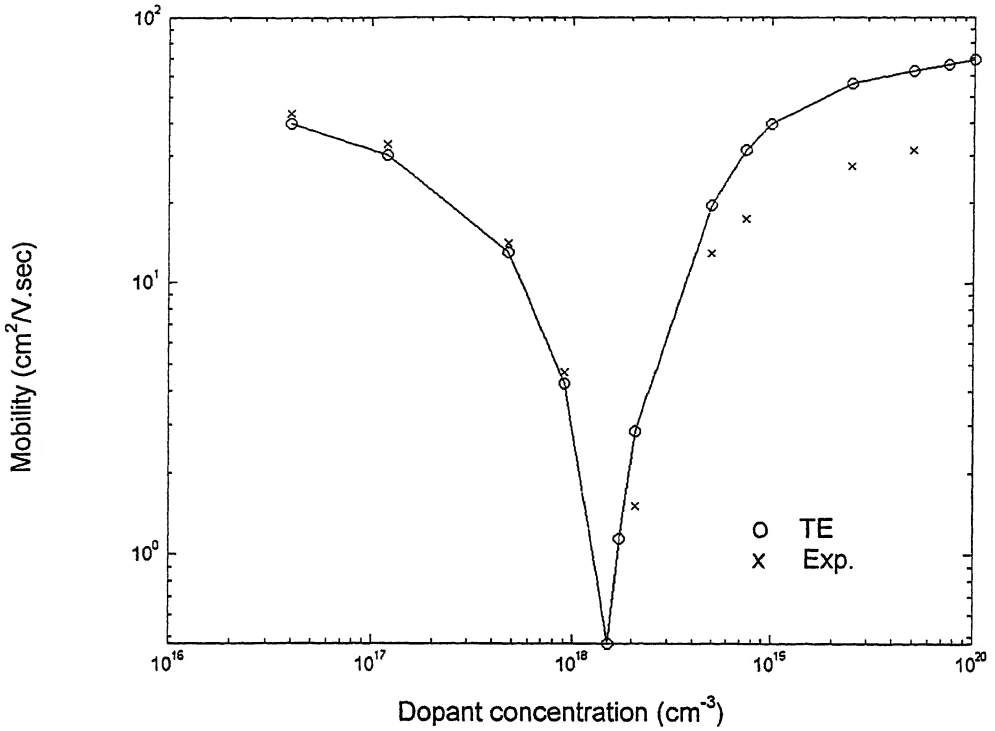

Figure 9a: Mobility Vs. Concentration for TE and Experimental Values L= 200A°

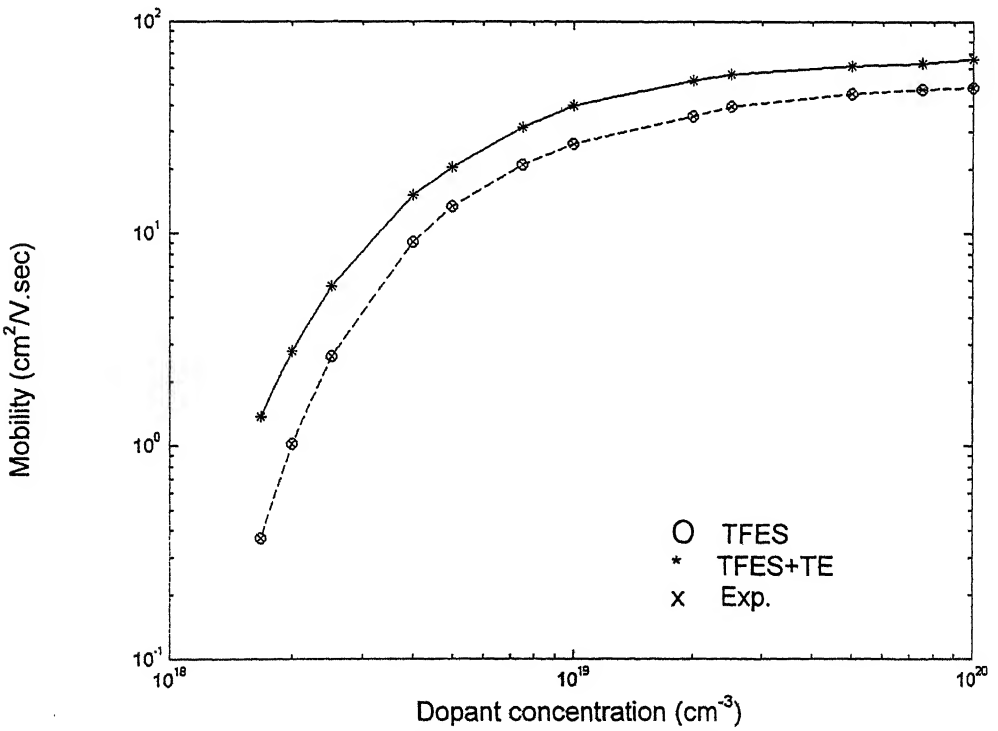

Figure 9b: Mobility Vs. Concentration for TE+TFES, TFES, and Experimental Value, L=200A°

S.No	Dopant Concentration $[cm^{-3}]$	For Grain Size= $200A^{o}$			
		Experimental Mobility $[cm^{-2}V^{-1}\sec^{-1}]$ [2]	TFES+TE Mobility $[cm^{-2}V^{-1}\sec^{-1}]$	TFES Mobility $[cm^{-2}V^{-1}\sec^{-1}]$	TE Mobility $[cm^{-2}V^{-1}\sec^{-1}]$
	$1.00X10^{16}$				45.70882
	$3.98X10^{16}$	52.48075			39.81072
	$1.20X10^{17}$	41.68694			30.19952
	$4.79X10^{17}$	16.2181			12.8825
	$9.12X10^{17}$	5.4881			4.265795
	$1.58X10^{18}$				0.4749
	$1.67X10^{18}$		1.36901	0.36901	1.148154
	$2.00X10^{18}$	1.230269	2.7592	1.023293	2.844461
	$5.00X10^{18}$		5.623413	2.630268	19.6336
	$7.50X10^{18}$		15.13561	9.120108	31.62278
	$1.00X10^{19}$	15.4257	20.41738	13.4257	39.81072
	$2.50X10^{19}$	23.09	31.62278	21.0901	56.23413
	$5.00X10^{19}$		39.81072	26.433	63.09573
	$7.50X10^{19}$		52.48075	35.48134	66.06934
	$1.00X10^{20}$	41.6892	56.23413	39.6892	69.1831

Table 7: Concentration and Mobilities due to different effects

4.2.3 Plots and Corresponding Data of "Mobility Vs Doping Concentration" For TFES+TE, TFES, TE and Experimental Values (1220A°Grain Size).

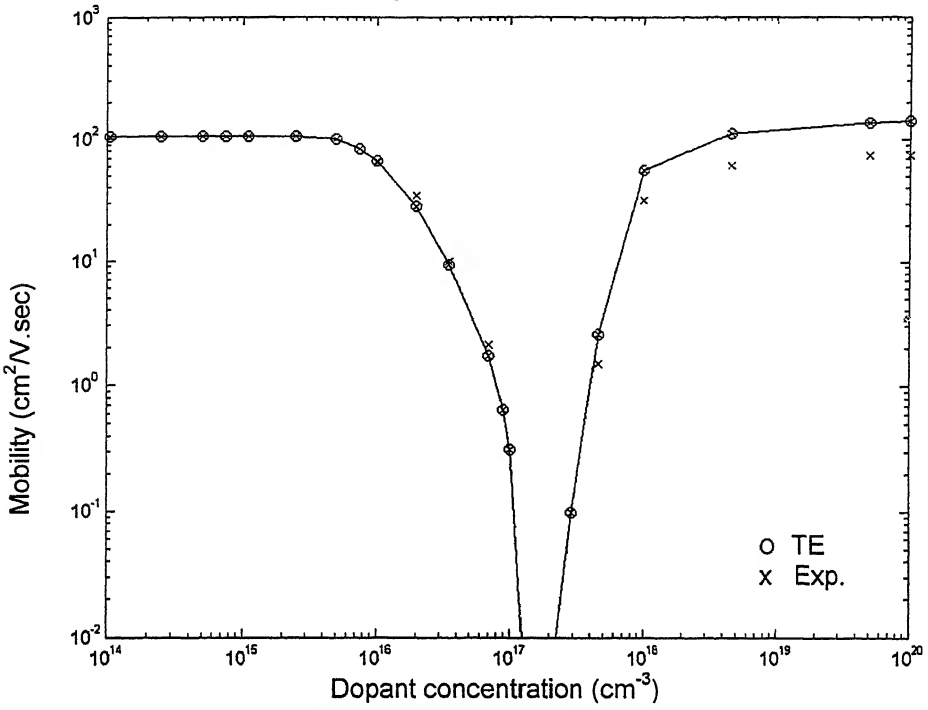

Figure 10a: Mobility Vs Concentration for TE+TFES, TFES, and Expt. Values for L=1220A^o

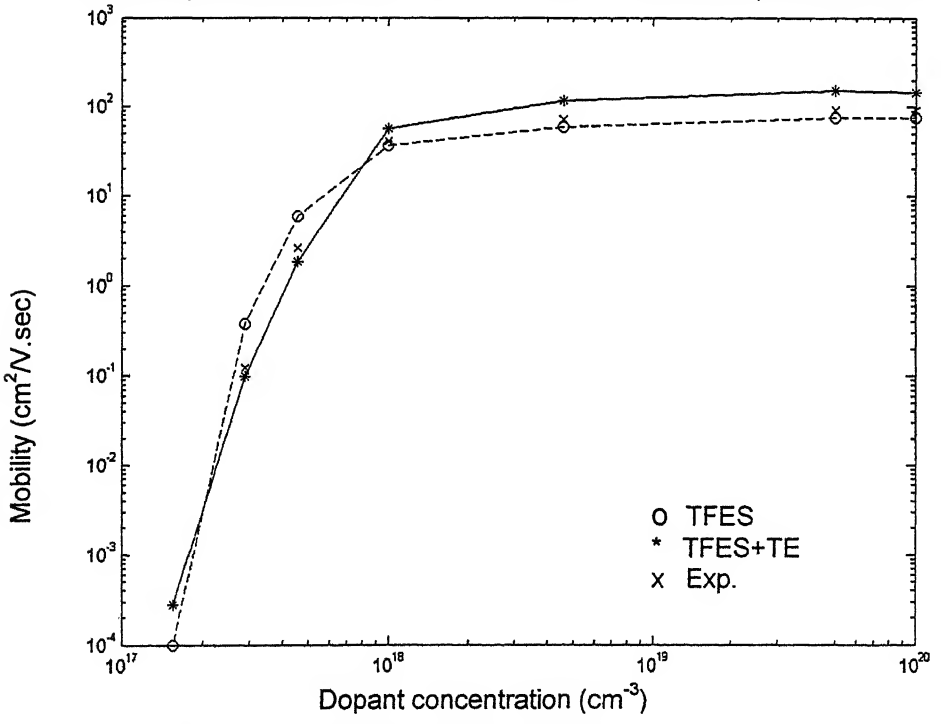

Figure 10b: Mobility Vs Concentration for TE+TFES, TFES, and Expt. Values for L=1220A^o

S.No	Dopant Concentration $[cm^{-3}]$	For Grain Size=1220A^o			
		Experimental Mobility $[cm^{-2}V^{-1}\sec^{-1}]$ [21]	TFES+TE Mobility $[cm^{-2}V^{-1}\sec^{-1}]$	TFES Mobility $[cm^{-2}V^{-1}\sec^{-1}]$	TE Mobility $[cm^{-2}V^{-1}\sec^{-1}]$
	$1.00X10^{16}$	64.28590			66.2859
	$2.00X10^{16}$	34.67369			28.0361
	$3.50X10^{16}$	10.54090			9.332543
	$7.00X10^{16}$	2.137962			1.737801
	$9.00X10^{16}$				0.645654
	$1.00X10^{17}$				0.316228
	$1.55X10^{17}$		0.000278	0.0001	0.000278
	$2.88X10^{17}$	0.123027	0.097724	0.380189	0.097724
	$4.57X10^{17}$	2.630268	1.819701	5.888437	2.570396
	$1.00X10^{18}$	40.73803	56.23413	36.30781	56.23413
	$4.60X10^{18}$	72.4436	117.4898	58.88437	112.2018
	$5.00X10^{19}$	91.20108	151.3561	75.85776	138.0384
	$1.00X10^{20}$	91.20108	144.544	75.85776	141.2538

Table 8: Concentration and Mobilities due to different effects

4.2.4 Plot and Corresponding Data of "Mobility Vs Temperature"

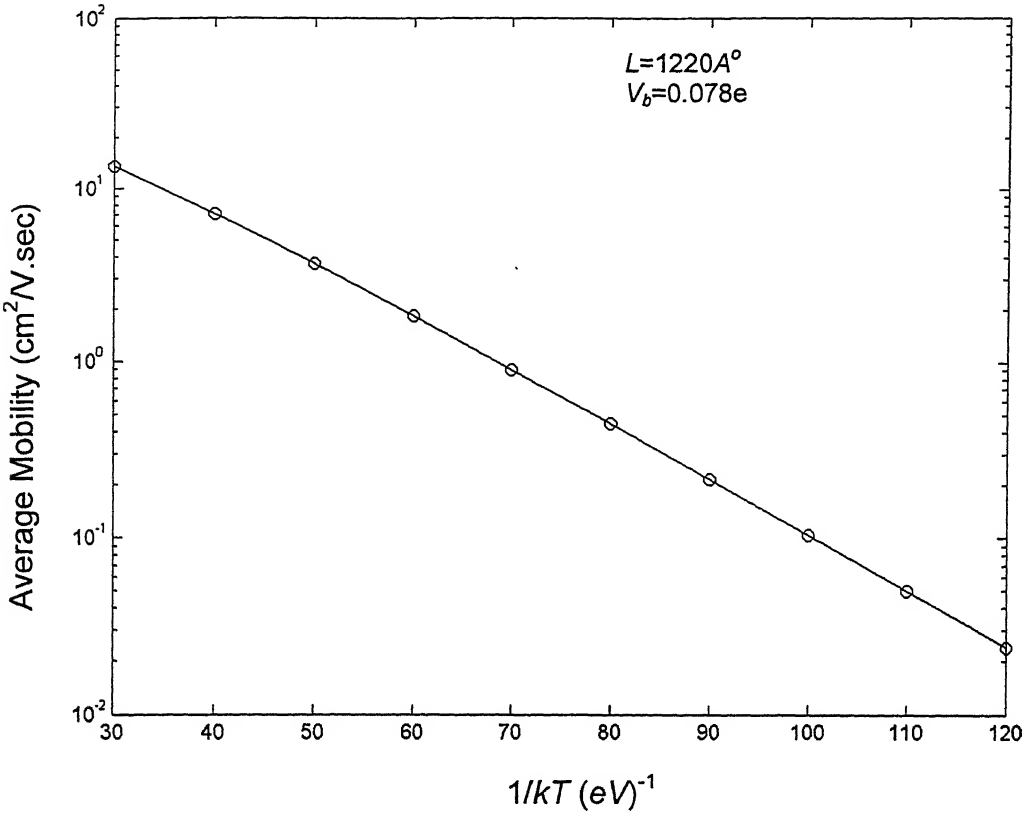

Figure 11: Mobility Vs. Inverse Temperature

S.No.	$1/kT\ (eV)^{-1}$	Average Mobility ($cm^2/V.sec$)
1	30	13.4713
2	40	7.1306
3	50	3.6545
4	60	1.8352
5	70	0.9087
6	80	0.4453
7	90	0.2165
8	100	0.1046
9	110	0.0503
10	120	0.0241

Table 9: Inverse Temperature and Average Mobility

4.2.5 Plots and Corresponding Data of "Doping Concentration Vs Average Carrier Concentration"

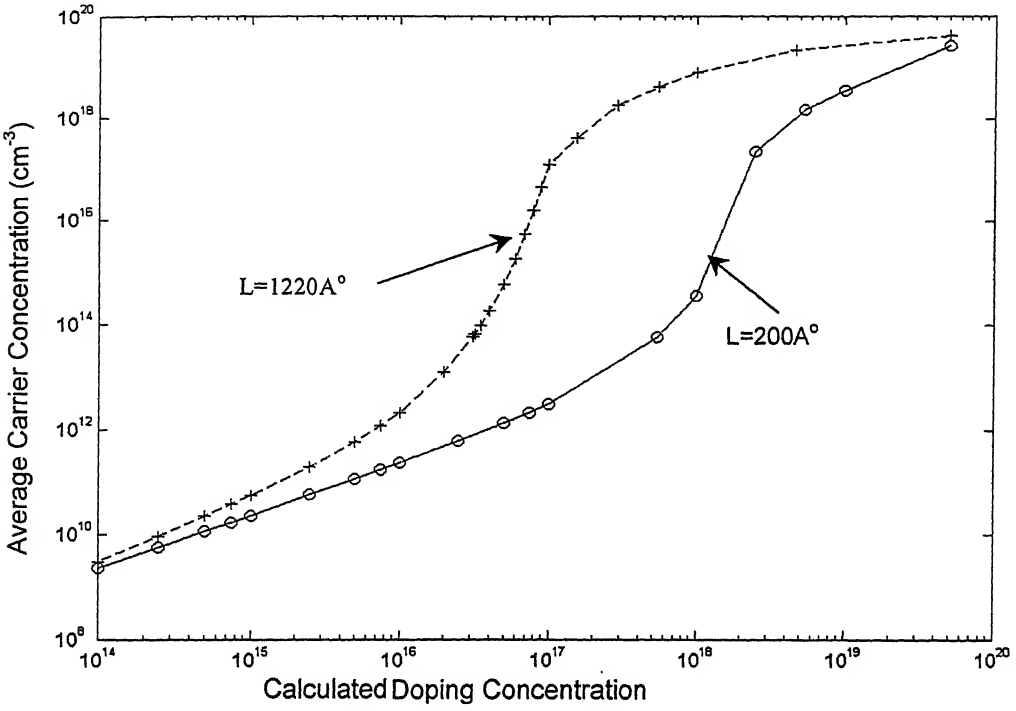

Figure 12a: Average Carrier Concentration Vs. Doping Concentration

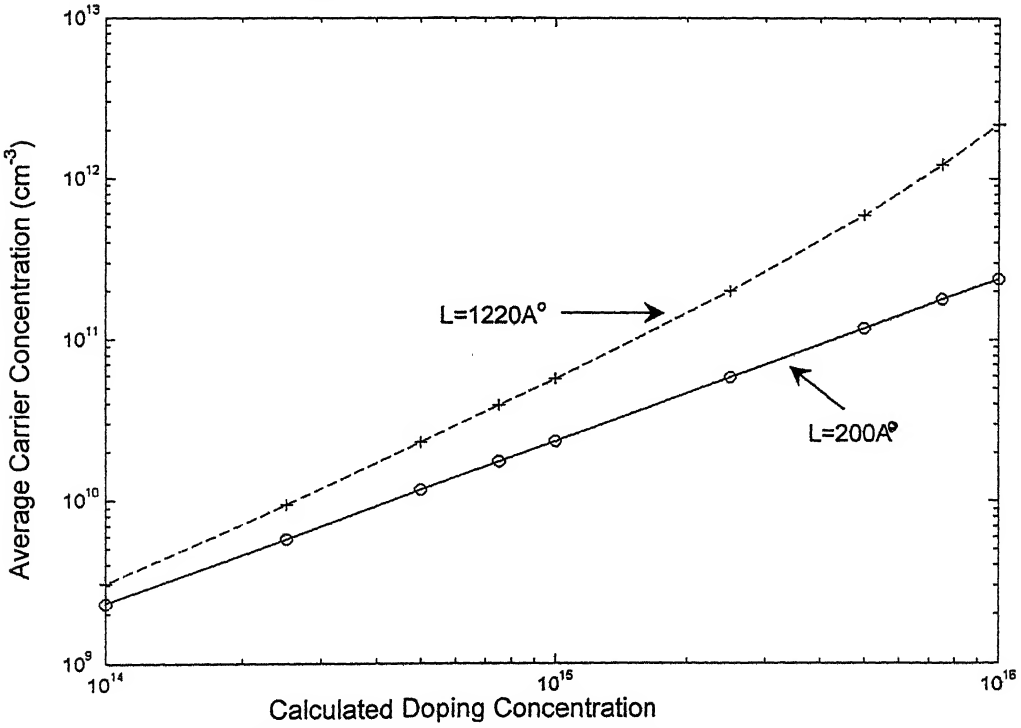

Figure 12b: Average Carrier Concentration Vs. Doping Concentration at Low Doping level

S.No.	Grain Size = 1220A^o		Grain Size = 200A^o	
	Doping Concentration (cm^{-3})	Average Carrier Concentration (cm^{-3})	Doping Concentration (cm^{-3})	Average Carrier Concentration (cm^{-3})
1.	$1.0x10^{14}$	$3.0764x10^{9}$	$1.0x10^{14}$	$2.332\ x10^{9}$
2.	$2.5\ x10^{14}$	$9.409\ x10^{9}$	$2.5\ x10^{14}$	$5.80\ x10^{9}$
3.	$5.0\ x10^{14}$	$2.309\ x10^{10}$	$5.0\ x10^{14}$	$1.1162\ x10^{10}$
4.	$7.5\ x10^{14}$	$3.889\ x10^{10}$	$7.5\ x10^{14}$	$1.744\ x10^{10}$
5.	$1.0x10^{15}$	$5.666\ x10^{10}$	$1.0x10^{15}$	$2.327\ x10^{10}$
6.	$2.5\ x10^{15}$	$2.0027x10^{11}$	$2.5\ x10^{15}$	$5.846\ x10^{10}$
7.	$5.0\ x10^{15}$	$5.88\ x10^{11}$	$5.0\ x10^{15}$	$1.1781\ x10^{11}$
8.	$7.5\ x10^{15}$	$1.22\ x10^{12}$	$7.5\ x10^{15}$	$1.781\ x10^{11}$
9.	$1.0\ x10^{16}$	$2.17\ x10^{12}$	$1.0\ x10^{16}$	$2.392\ x10^{11}$
10.	$2.0\ x10^{16}$	$1.25\ x10^{12}$	$2.5\ x10^{16}$	$6.253\ x10^{11}$
11.	$3.1\ x10^{16}$	$5.824\ x10^{13}$	$5.0\ x10^{16}$	$1.3471\ x10^{12}$
12.	$3.2\ x10^{16}$	$6.628\ x10^{13}$	$7.5\ x10^{16}$	$2.1764\ x10^{12}$
13.	$3.5\ x10^{16}$	$9.706\ x10^{13}$	$1.0\ x10^{17}$	$3.1252\ x10^{12}$
14.	$4.0\ x10^{16}$	$1.797\ x10^{14}$	$5.54\ x10^{17}$	$5.9499\ x10^{13}$
15.	$5.0\ x10^{16}$	$5.839\ x10^{14}$	$1.0\ x10^{18}$	$3.5398\ x10^{14}$
16.	$6.0\ x10^{16}$	$1.8\ x10^{15}$	$2.5\ x10^{18}$	$2.2694\ x10^{17}$
17.	$7.0\ x10^{16}$	$5.39\ x10^{15}$	$5.4\ x10^{18}$	$1.4835\ x10^{18}$
18.	$8.0\ x10^{16}$	$1.56\ x10^{16}$	$1.0x10^{19}$	$3.5989\ x10^{18}$
19.	$9.0\ x10^{16}$	$4.475\ x10^{16}$	$5\ .0x10^{19}$	$2.5778\ x10^{19}$
20.	$1.0\ x10^{17}$	$9.26\ x10^{16}$		
21.	$1.55\ x10^{17}$	$1.20\ x10^{17}$		
22.	$2.88\ x10^{17}$	$1.819\ x10^{17}$		
23.	$5.46\ x10^{17}$	$4.155\ x10^{17}$		
24.	$1.0\ x10^{18}$	$7.883\ x10^{17}$		
25.	$4.64\ x10^{18}$	$2.1427\ x10^{18}$		
26.	$5.0\ x10^{19}$	$4.063\ x10^{19}$		

Table 10: Doping Concentration and Average Carrier Concentration

4.2.6 Plots and Corresponding Data of "Resistivity vs. Doping Concentration" For TFES+TE, TFES, TE and Experimental Values (200A°Grain size).

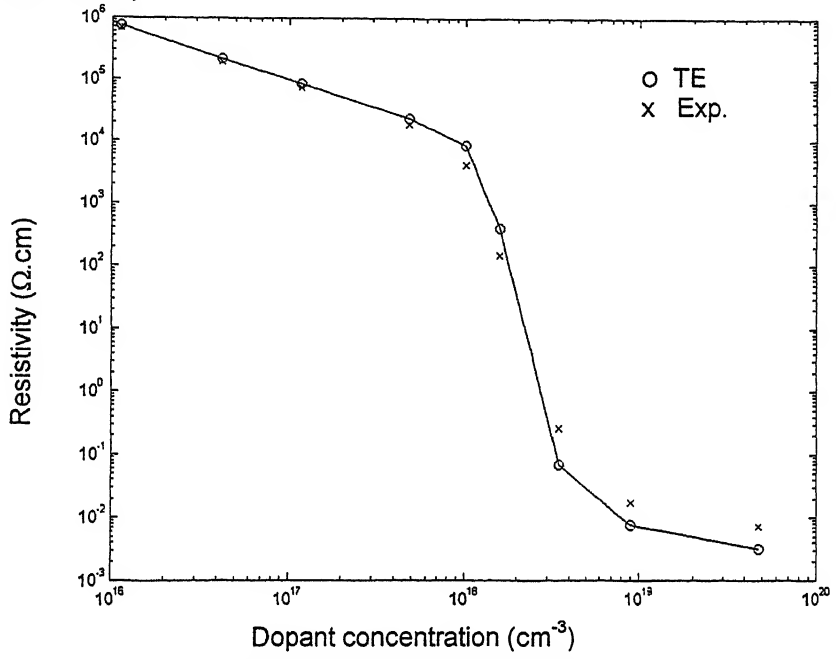

Figure 13a: Resistivity Vs Doping concentration for TE and Experimental Values for L=200A°

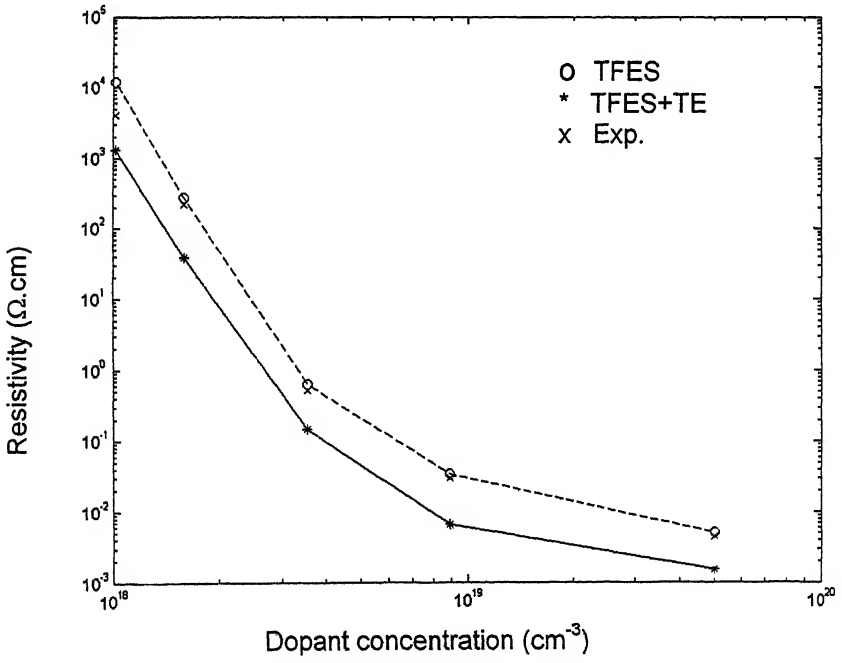

Figure 13b: Resistivity Vs Doping concentration for TFES+TE, TFES and Experimental Values

S.No	Dopant Concentration $[cm^{-3}]$	For Grain Size= $200A^{o}$			
		Experimental Resistivity $[\Omega.cm]$ [2,7]	TFES+TE Resistivity $[\Omega.cm]$	TFES Resistivity $[\Omega.cm]$	TE Resistivity $[\Omega.cm]$
1.	$1.1220X10^{16}$	$6.9183X10^{05}$			$7.41000X10^{05}$
2.	$4.1687X10^{16}$	$1.9055X10^{05}$			$2.14000X10^{05}$
3.	$1.1749X10^{17}$	$7.4131X10^{04}$			$8.3200X10^{04}$
4.	$4.7863X10^{17}$	$1.8197X10^{04}$			$2.2900X10^{04}$
5.	$9.1201X10^{17}$	$4.0738X10^{03}$			$8.5100X10^{03}$
6.	$1.5849X10^{18}$	$1.4454X10^{02}$	$1.3183X10^{03}$	$1.2000X10^{04}$	$3.8905X10^{02}$
7.	$3.4674X10^{18}$	$2.5704X10^{-01}$	$3.8905X10^{01}$	$2.7542X10^{02}$	$6.9183X10^{-02}$
8.	$8.9125X10^{18}$	$1.7378X10^{-02}$	$1.4791X10^{-01}$	$6.3096X10^{-01}$	$7.5858X10^{-03}$
9.	$5.0000X10^{19}$	$7.0795X10^{-03}$	$6.6069X10^{-03}$	$3.3884X10^{-02}$	$3.1623X10^{-03}$

Table 11: Concentration and Resistivity due to different effects.

4.2.7 Plots and Corresponding Data of "Resistivity vs. Doping Concentration" For TFES+TE, TFES, TE and Experimental Values (1220A°Grain size)

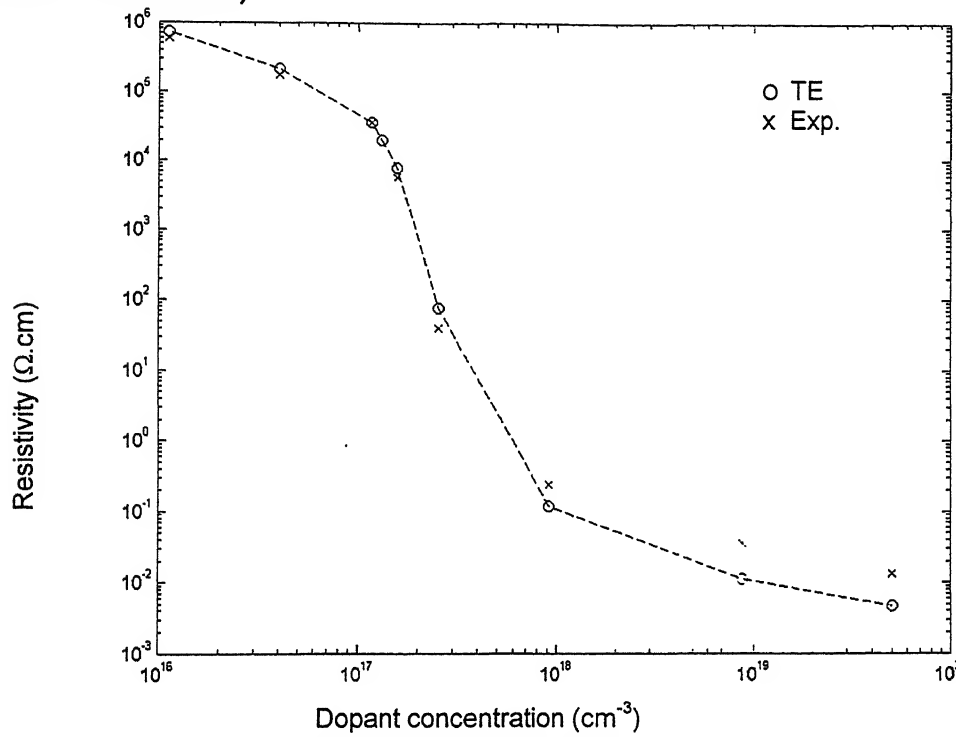

Figure 14a: Resistivity Vs Doping concentration for TE, and Experimental Values,L=1220A°

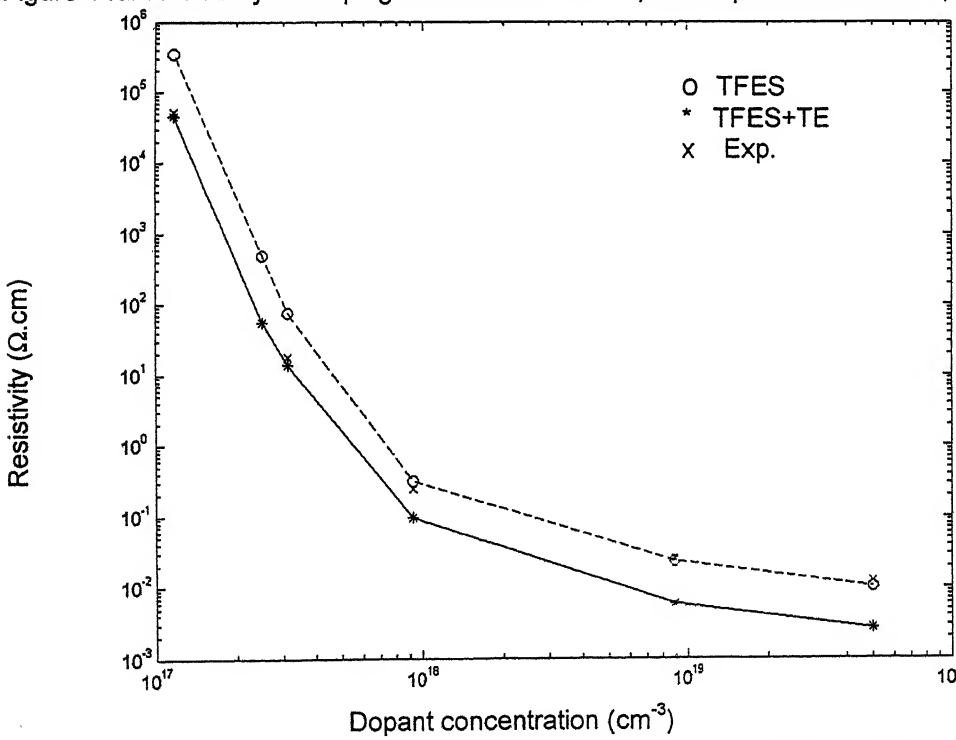

Figure 14b: Resistivity Vs Doping concentration for TFES+TE, TE and Experimental Values

S.No	Dopant Concentration $[cm^{-3}]$	For Grain Size=1220A^{o}			
		Experimental Resistivity $[\Omega.cm]$[7,20]	TFES+TE Resistivity Only $[\Omega.cm]$	TFES Resistivity $[\Omega.cm]$	TE Resistivity $[\Omega.cm]$
	1.1220X1016	$4.1687X10^{05}$			$7.2400X10^{05}$
	3.9811X1016	$1.2589X10^{05}$			$2.1400X10^{05}$
	1.1749X1017	$5.2481X10^{04}$	$4.4668X10^{04}$	$3.4700X10^{05}$	$3.6300X10^{04}$
	2.4946X1017		$5.4954X10^{01}$	$4.9000X10^{02}$	$7.7600X10^{03}$
	3.1261X1017	$1.8197X10^{01}$	$1.3804X10^{01}$	$7.5858X10^{01}$	$7.5858X10^{01}$
	9.2683X1017	$2.4547X10^{-01}$	$9.5499X10^{-02}$	$3.1623X10^{-01}$	$1.1749X10^{-01}$
	8.9125X1018	$2.5704X10^{-02}$	$5.8884X10^{-03}$	$2.3442X10^{-02}$	$1.1220X10^{-02}$
	5.0000X1019	$1.2303X10^{-02}$	$2.6303X10^{-03}$	$1.0233X10^{-02}$	$4.6774X10^{-03}$

Table 12: Concentration and Resistivities due to different effects.

4.2.8 Plot and Corresponding Data of "Resistivity vs. Doping Concentration" for Different Grain Sizes (200A°-1220A°)

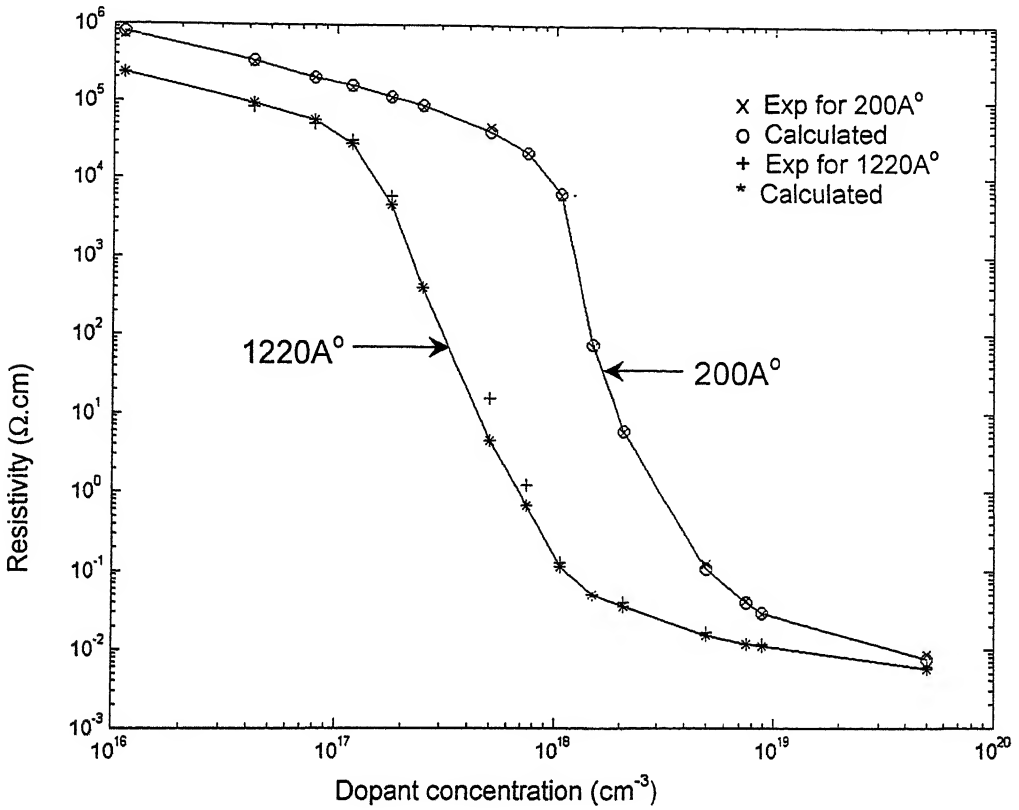

Figure 15a: Resistivity Vs doping concentration for different grain size

S.No	Dopant Concentration $[cm^{-3}]$	Grain Size= $200A^{o}$		Grain Size= $1220A^{o}$	
		Experimental Resistivity $[\Omega.cm]$ [2,20]	Calculated Resistivity $[\Omega.cm]$	Experimental Resistivity $[\Omega.cm]$ [7,20]	Calculated Resistivity $[\Omega.cm]$
	1.1220X10^{16}	7.2444X10^{05}	7.7600X10^{05}	2.3442X10^{05}	2.3442X10^{05}
	3.9811X10^{16}	3.1623X10^{05}	3.3900X10^{05}	8.5114X10^{04}	8.3176X10^{04}
	1.1749X10^{17}	1.5136X10^{05}	1.6200X10^{05}	3.1623X10^{04}	2.8184X10^{04}
	4.7863X10^{17}	1.1220X10^{05}	1.1500X10^{05}	5.8884X10^{03}	4.5709X10^{03}
	9.1201X10^{17}	8.5114X10^{04}	8.9100X10^{04}	4.0738X10^{02}	3.9811X10^{02}
	1.5849X10^{18}	9.1201X10^{03}	9.7724X10^{03}	1.2882X10^{-01}	1.1482X10^{-01}
	3.4674X10^{18}	4.7542X10^{00}	5.8884X10^{00}	3.9811X10^{-02}	3.5481X10^{-02}
	8.9125X10^{18}	2.8184X10^{-02}	2.5119X10^{-02}	1.2023X10^{-02}	1.1220X10^{-02}
	5.0000X10^{19}	8.7096X10^{-03}	7.5858X10^{-03}	6.0256X10^{-03}	5.7544X10^{-03}

Table 13: Concentration and Resistivities for Different Grain Size

4.2.9 Plot and Corresponding Data of "Grain Size Vs Resistivity"

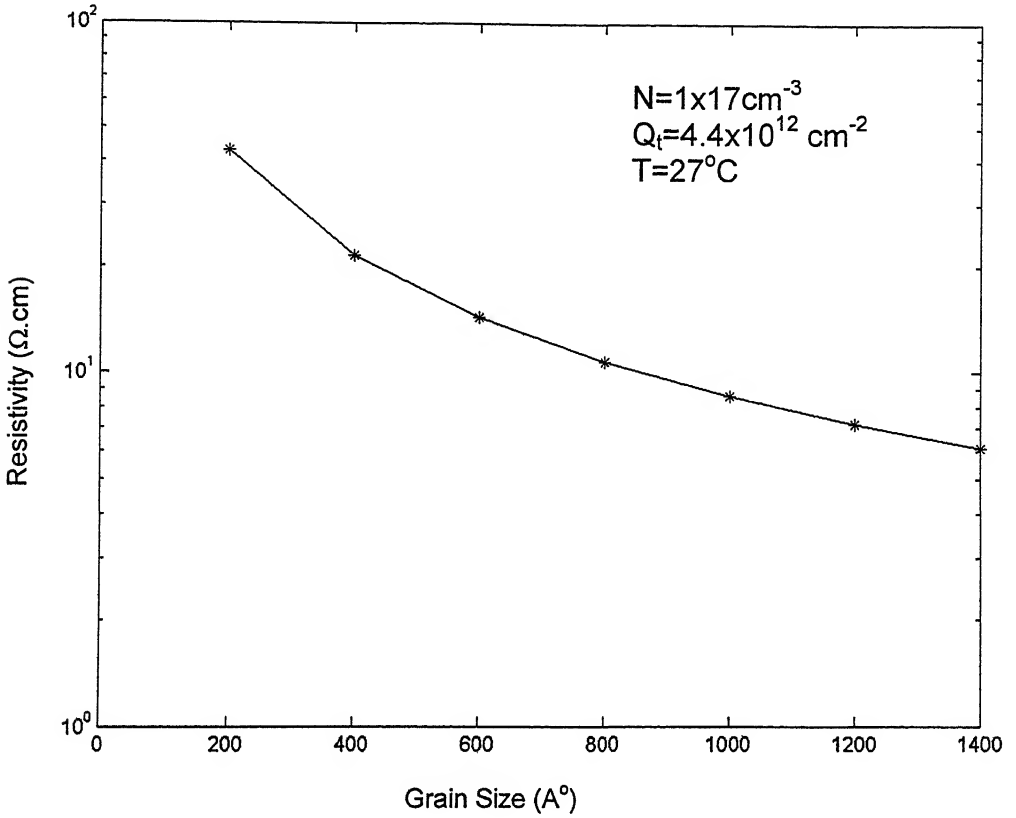

Figure 15b: Resistivity Vs. Grain Size

S.No.	Grain Size (A°)	Resistivity (Ω. cm)
1.	200	42.9004
2.	400	21.4502
3.	600	14.3001
4.	800	10.7251
5.	1000	8.5801
6.	1200	7.1501
7.	1400	6.1286

Table 14: Grain Size and Resistivity

4.2.10 Plot and Corresponding Data of "Current Density Vs Voltage (J-V) Plot"

Current density Vs voltage characteristic is drawn using both TFES and TE, i.e. their combined relation given equation (43a),

$$J = q^2 N_G \left(\frac{1}{2\pi m_h^* kT} \right)^{1/2} e^{-qV_b/kT} V_o$$

V_o is the applied voltage across the composite grain boundary region. If the applied voltage is V_a and the number of grains are g.

$$\therefore V_o = \frac{V_a}{g}$$

$$J = q^2 N_G \left(\frac{1}{2\pi m_h^* kT} \right)^{1/2} e^{-qV_b/kT} \frac{V_a}{g}$$

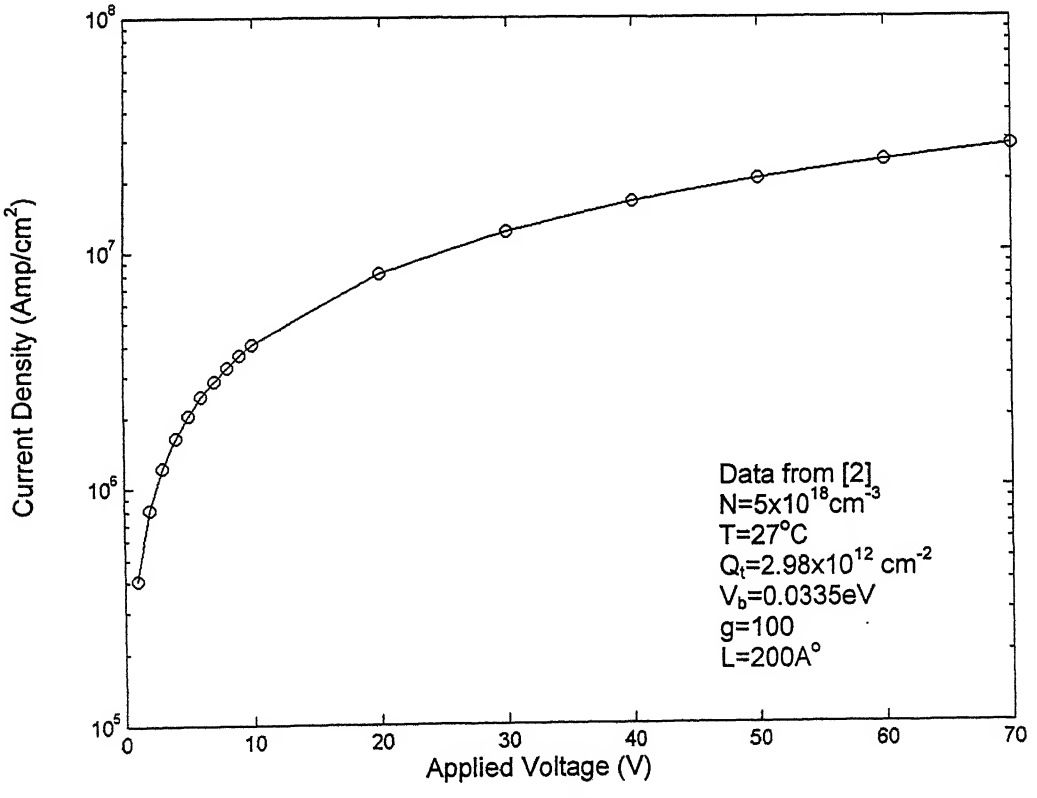

Figure 16: Current Density Vs. Voltage at Room Temperature

S.No.	Voltage (V)	Current Density (Amp.cm^{-2}) x10^{7}
1.	1	.0407
2.	2	0.0815
3.	3	0.1222
4.	4	0.1629
5.	5	0.2036
6.	6	0.2444
7.	7	0.2851
8.	8	0.3258
9.	9	0.3665
10.	10	0.4073
11.	20	0.8145
12.	30	1.2218
13.	40	1.6291
14.	50	2.0363
15.	60	2.4436
16.	70	2.8509

Table 15: Voltage and Current Density

Chapter 5

Analysis And Discussion

5.1 Discussion About Grain Boundary

The theoretical model was matched to experimental data (Table 1-4) using the width of the grain –boundary barrier, W_{gb}, as fitting parameter. W_{gb} is determined by using Newton-Raphson iterative method. The value of W_{gb} comes out to be $11.86A^0$ at trapping density 3.34×10^{12} cm^{-2} (Table 1) and at very high doping concentration it comes out to be 11.89 A^0 (Table 3). It should be noted here that the value for the W_{gb} is physically reasonable. A grain-boundary height of 0.66 eV gives a grain boundary band gap of 1.32eV, which satisfies the basic assumption of the model. A grain boundary thickness of $11.86A^o$ or 11.89 A^o is roughly the width of two –three mono layers, which seems to be reasonable when compared to grain boundary width of $7A^o$ in case of phosphorous doped polysilicon[4]. Grain boundary is the transitional region separating the highly ordered crystallites. The grain boundary width is different for P, & As [4] as compared to B, hence it can be concluded that grain boundary width is the property of dopant species. It is also seen that, both at moderate and high doping concentration there is not a significant change in the W_{gb}, implying that it is not a function of dopant concentration as well.

5.2 Discussion of Various plots

1. In section 4.2.1, Figure (7), plot of barrier height vs. doping concentration is shown; the barrier height increases with doping concentration and after reaching a maximum value starts decreasing. It is due to the fact that

barrier height varies differently with doping concentration at low and high doping concentrations respectively. When the doping concentration is lower than the trapping density ($LN<Q_t$), the crystallite is completely depleted of carrier and the traps are partially filled. According to Seto [2] Barrier height (V_b) increases linearly with doping concentration. Linear variation is given by,

$$V_b = \frac{qNL^2}{8\varepsilon}$$

where N is the doping concentration.

Seto [2] assumed that grains are completely depleted at low doping concentration, which is possible only at very low doping concentration not at moderate doping. Therefore the relation (2W=L) distorts the linear variation at low doping concentration as shown in plot of Figure (7)

When all the traps are filled ($LN>Q_t$), only part of the crystallite is depleted of carriers. V_b varies inversely with doping concentration, thereby decreasing the V_b at high doping concentrations.

$$V_b = \frac{qQ_t^2}{8\varepsilon N}$$

Our plot shows the same potential barrier values as shown in [21,22] experimentally.

Figure (8a) shows the plot between Mobility Vs doping concentration. Since the Mobility depends on the negative exponential of V_b (equation 43c), therefore, when the V_b increases mobility decreases. Our results are similar to that in [2,21]. Value of mobility at very low doping concentration is shown in Figure (8a), we see that curve is almost flat, that means at very low doping concentration there is not appreciable change in mobility.

Figure (8b, 8c) shows that contribution due to thermionic emission deviate from the effective mobility value at high dopant concentration. These plots also show that effective mobility value reaches to single crystal range at high dopant concentration. The reason is clear from equation (39) as thermionic mobility is very high so its reciprocal is negligible compare to

single crystal. Therefore, mobility at high dopant concentration is approximately in single crystal range. This result is same as given in [21]. In sections 4.2.2 Figure (9a, 9b) and in section 4.2.3 Figure (10a, 10b) plots of mobility Vs doping concentration are shown and a comparison is shown between (TFES+TE), TFES, TE and the experimental values for two different grain sizes 200A° and 1220A° respectively. We analyze that at low doping concentration thermionic emission (TE) matches with experimental values. In section 3.3.2 reason is given why at low doping concentration TE dominates. At high doping concentration (10^{17}-10^{18}) contribution of (TFES+TE) matches with the experiments (Figure 9-10). But as the concentration increases (10^{18}-10^{20}) contribution due to TFES increases significantly The reason is clear from the fact that all our assumptions are satisfied at high dopant concentration. Similar results are obtained for both low and high grain sizes. Better results are obtained in case of higher grain size. Our results predict the same conclusion as given in [2,7,20,21,24].

2. In section 4.2.4, Figure (11), plot of mobility as a function of ($1/kT$) is shown, based on empirical equation (43f), which shows a straight-line behavior with negative slope equal to the barrier height (qV_b). Plot is drawn at barrier height 0.078V, grain size $1220A^o$ and doping concentration $8.92x10^{17}cm^{-3}$. Figure (11) is provided for making the comparison with the values obtained from the empirical relation.
3. In section 4.2.5, Figure (12a, 12b), shows the plots between doping concentration Vs active carrier concentration. We know that at low doping concentration majority of the carriers are trapped in the grain boundary; hence the active carrier concentration is very small in comparison to the doping concentration. When all the traps are filled majority of the carriers contribute to the conduction. Therefore active carrier concentration increases at high dopant concentration as shown in the Figure (12a). At very high doping concentration active carrier concentration is almost same as doping concentration. We see in the Figure (12a, 12b), that there is a

increase in active carrier concentration between doping range ~10^{17} - $2x10^{18}$. This is result of the fact that as traps gets nearly filled more & more dopant atoms contribute to the free carriers. Further increase in dopant concentration reduces the depletion layer and eventually the free carrier contribution approaches that of crystalline silicon this is also in agreement with results in [2] and [21].

4. In section 4.2.6, Figures (13a, 13b), and in section 4.2.7, Figures (14a, 14b), show the plots between resistivity Vs doping concentration for low as well as high grain sizes. The contribution due to TE, TFES, (TFES+TE) is compared to the experimental values. At low doping concentration plot of TE alone matches with the experimental values. At the high doping concentration (10^{17}-10^{18}) contribution of (TFES+TE) matches with the experimental values, while TE considered alone deviates. But as the concentration is further increased from (10^{18}-10^{20}) contribution of TFES increases significantly. Therefore in this range contribution of TFES alone matches with Experimental Values (Figure 13-14). We got similar results as shown in [2,7,20]. Thus we see that resistivity cannot be explained using a single mechanism of transport. It is governed by different phenomenon at low and high doping concentration. These results give the conclusion that TE is dominant phenomenon at low doping concentration and TFES is a dominating phenomenon at very high doping concentration.

   We see in Figures (13-14) that at low doping concentration resistivity is very high then an abrupt change occurs in resistivity between doping range 10^{17}-10^{18} (L=1220A°) and 10^{18}-10^{19} (L=200A°) after that resistivity decreases approximately linearly. The reason of sharp decrease in resistivity is clear from the discussion above that under this range number of free carrier increases abruptly, consequently resistivity decreases .The reason of high resistivity at low doping concentration is that, most of the carriers are trapped leaving only a few free to contribute to the conduction. Carrier trapping results in the reduction in the number of free

carriers within the grains. Hence resistivity is very high at low doping concentration At high doping concentration (10^{18}-10^{19}) the resistivity reaches to single crystal range as illustrated by Table 5.

In section 4.2.8, Figure (15a), plots of resistivity Vs doping concentration for grain sizes $200A^{o}$and $1220A^{o}$ are shown. We get the lower values of resistivity for higher grain size. Similarly in section 4.2.9 Figure (15b) plot of resistivity Vs different grain size is shown, resistivity decreases with increasing gain size. Reason of lower value for higher grain size is obvious from equation (42b, 43d), resistivity is inversely proportional to the grain size.

5. In section 4.2.10 Figure (16) plot of current density Vs voltage is shown using equation (43a), Numbers of grains are taken 100 from Baccarani [22]. We got a similar hyperbolic sine J-V curve as shown in [5,20,22,]. Equation (43a) can be used to calculate the number of grain.

Chapter 6

Conclusions

This work was carried out to study the electronic properties of boron doped polysilicon films. This material has drawn considerable attention for its potential application in polysilicon devices namely n-channel thin films transistors (TFT s). The objective of the studies was to have better understanding of electronic properties of the material namely mobility, conductivity (resistivity), transport mechanism in general and how the free carrier concentration varies as a function of doping levels in the material.

The study concludes that for fine grain Boron doped polysilicon (grain size 200-1220A°), at high doping concentration ($\geq 10^{18}$ cm^{-3}), most of the dopants contribute to free carriers. However, at lower doping concentration only a fraction of the dopants contribute to average carriers. This result, though previously reported by other researchers up to 10^{16} cm^{-3}, did not cover the doping range as low as $10^{14}cm^{-3}$. The study shows that at doping concentration of 10^{14} cm^{-3}, the free carrier concentration is $\sim 10^{9}cm^{-3}$. Similar results were obtained for 200A° and 1220A° grain sizes.

The study also concludes that at low dopant concentration ($<10^{17}cm^{-3}$) Thermionic emission (TE) is the dominant mechanism behind carrier transport across the grain boundaries. However, both thermionic emission (TE) and thermionic field emission with scattering (TFES) contribute to carrier transport across the grain boundaries at high doping concentration (10^{17}-$10^{18}cm^{-3}$). Further, at very high doping concentration TFES is the dominant mechanism of transport across the grain boundaries.

The study also shows that resistivity decreases with increasing grain size, which is in general agreement with the works of others.

Scope for the future work

In the present work assumption has been made that the applied voltages is less than kT/q, so that in addition to thermionic emission carriers tunnel through the grain boundaries. However, at high voltage TFE may also contribute to the conduction mechanism and must be considered.

Appendix A

Potential Barrier Equation

Writing the Poisson's equation for depleted grain

$$\frac{d^2V(x)}{dx^2} = \frac{qN}{\varepsilon}$$

On integration,

$$\frac{dV(x)}{dx} = \frac{qN}{\varepsilon}x + c_1$$

After applying the boundary condition at $x = W + \frac{W_{gb}}{2}, \frac{dV(x)}{dx} = 0$ as the field is zero in the neutral region.

$$\frac{dV(x)}{dx} = \frac{qN}{\varepsilon}\left[x - \left(W + \frac{W_{gb}}{2}\right)\right]$$

Again integrating we get,

$$V(x) = \frac{qN}{2\varepsilon}\left[x - \left(W + \frac{W_{gb}}{2}\right)\right]^2 + c_2$$

Now at $x = \frac{W_{gb}}{2}, V(x) = V_b$

$$V(x) = \frac{qN}{2\varepsilon}\left[x - \left(W + \frac{W_{gb}}{2}\right)\right]^2 + \left(V_b - \frac{qNW^2}{2\varepsilon}\right)$$

.At x=0 the first term on the right hand side of the above equation becomes zero and potential is also zero.

Therefore,

$$V_b = \frac{qNW^2}{2\varepsilon}$$

So finally we have,

$$V(x) = \frac{qN}{2\varepsilon}\left[\left(W + \frac{W_{gb}}{2}\right) - |x|\right]^2 \text{ For } \frac{W_{gb}}{2} < |x| < \left(W + \frac{W_{gb}}{2}\right)$$

At low doping concentration grains are completely depleted, so $2W = L$.

$$V_b = \frac{qNL^2}{8\varepsilon}$$

Appendix B

W.K.B Method

This method applies only situations in which the potential is slowly varying function of position.

Let $\Psi(x)$ be the wave function satisfying Schroedinger`s equation.

$$\frac{\delta^2\Psi}{\delta x^2}+\frac{2m}{\hbar^2}[E-qV(x)]\Psi=0 \tag{1}$$

again, f the solution of equation (1) be in the from $\Psi = Ce^{i\phi(x)/\hbar}$, then we get from equation (1).

$$i\hbar\phi''(x)-\phi'^2(x)+2m[E-qV(x)]=0 \tag{2}$$

To get the approximate solution of (2), we apply W.K.B method and hence expand $\phi(x)$ in powers of $\hbar$ i.e.

$$\phi(x)=\phi_0(x)+\hbar\phi_1(x)+\frac{\hbar^2}{2}\phi_2(x)+.... \tag{3}$$

as $\hbar$ is very small , the first two term in the above equation give sufficiently good approximation of $\phi(x)$. So putting the value of $\phi(x)$ in equation (2) and collecting coefficient of various power of $\hbar$. We get ,

$$2m[(E-qV(x))-\phi_0'^2]+\hbar\left[i\phi_0''-2\phi_0'\phi_1'\right]+\hbar^2\left[i\phi_1''-\phi_1'^2-\phi_0'\phi_2'\right]=0 \tag{4}$$

thus from equation (4) we get ,

$$\left.\begin{aligned}
&\phi_0' = \pm\sqrt{[2m(E-qV(x))]} \\
&\therefore \phi_0 = \pm\int_a^b \sqrt{[2m(E-qV(x))]}dx \\
&\phi_1 = \frac{i}{2}\ln\left|\phi_0'\right| + c_1 \\
&\phi_2 = \frac{m\left(\frac{\delta V}{\delta x}\right)}{2[2m(E-qV(x))]^{3/2}} - \frac{1}{4}\int_a^b \frac{m^2\left(\frac{\delta V}{\delta x}\right)dx}{[2m(E-qV(x)]^{5/2}}
\end{aligned}\right\} \quad (5)$$

We see that $\phi_2(x)$ will be small whenever $\frac{\delta V}{\delta x}$ is small and $[E-qV(x)]$ is not too close to zero.

$$\phi(x) \approx \phi_0(x) + \frac{i\hbar}{2}\ln\left|\phi_0'\right|$$

$$\Psi(x) = C[2m(E-qV(x))]^{-1/4}\exp\left[\pm\frac{i}{\hbar}\int_a^b\sqrt{[2m(E-qV(x))]}dx\right] \quad (6)$$

This $\pm$ show the direction of motion of the wave function in positive & negative direction.

We can write it in more compact from using the momentum expression.

$$p = \sqrt{2m(E-qV(x))}$$

$$\Psi(x) = \frac{C}{\sqrt{p}}\exp\left[\pm i\int_a^b \frac{p}{\hbar}dx\right] \quad (7)$$

$$Transmision\ \Pr obability(D)=\frac{TransmittedIntensity}{IncidentIntensity}$$

After solving transmitted intensity & incident intensity we get,

$$\left.\begin{aligned} Transmitte\ dIntensity &= \frac{|C|^2}{p} \\ IncidentIntensity &= \frac{|C|^2}{p}\left[\exp\left\{\int_a^b \frac{p}{\hbar}dx\right\}-\frac{1}{4}\exp\left\{\int_a^b \frac{-p}{\hbar}dx\right\}\right]^2 \end{aligned}\right\} \quad (8)$$

Under W.K.B approximation. $\int_a^b \frac{pdx}{\hbar} >> 1$

Thus;

$$\boxed{D=\exp\left\{\frac{-2}{\hbar}\int_a^b \sqrt{[2m(qV(x)-E)]}dx\right\}} \quad (9)$$

Appendix-C

Concentration Density

$$N(E_x) = \frac{2p_x dp_x}{h^3 m_h^*} \int_0^{2\pi} \int_0^{\infty} \frac{p_\rho dp_\rho d\theta}{\left[1 + \exp\left(\left(\frac{p_x^2 + p_\rho^2}{2m_h^*} - E_F\right) \Big/ kT\right)\right]} \tag{1}$$

Say

$$\frac{p_\rho^2}{2m_h^*} = \varepsilon_\rho$$

$$2p_\rho dp_\rho = d\varepsilon_\rho 2m_h^*$$

$$N(E_x) = \frac{2m_h^* p_x dp_x}{h^3 m_h^*} \int_0^{2\pi} \int_0^{\infty} \frac{d\varepsilon_\rho}{\left[1 + \exp\left(\left(\frac{p_x^2}{2m_h^*} + \varepsilon_\rho - E_F\right) \Big/ kT\right)\right]} \tag{2}$$

Solving the first integral.

$$N(E_x) = \frac{4\pi m_h^*}{h^3} \frac{p_x dp_x}{m_h^*} \int_0^{\infty} \frac{d\varepsilon_\rho}{\left[1 + \exp\left(\left(\frac{p_x^2}{2m_h^*} + \varepsilon_\rho - E_F\right) \Big/ kT\right)\right]} \tag{3}$$

Now for the tunneling to be occurring K.E of the holes should be lesser than Fermi energy.

$\therefore \frac{p_x^2}{2m_h^*} + \varepsilon_\rho < E_F$ So with this condition and

Say

$$y = \exp \frac{-\left(\frac{p^2}{2m_h^*} + \varepsilon_\rho - E_F\right)}{kT}$$

$$\therefore \frac{-dy}{y} = \frac{d\varepsilon_\rho}{kT}$$

$$N(E_x) = \frac{4\pi m_h^* kT}{h^3} \frac{p_x dp_x}{m_h^*} \int_{-\infty}^{e^{-\left(\frac{p_x^2}{2m_h^*} - E_F\right)}} \frac{dy}{y[1+y]}$$

$$N(E_x) = \frac{4\pi m_h^* kT}{h^3} \frac{p_x dp_x}{m_h^*} \left[\ln \frac{y}{(1+y)}\right]_{-\infty}^{e^{-\left(\frac{p_x^2}{2m_h^*} - E_F\right)}}$$

After solving & putting the proper limits,

$$N(E_x) = \frac{4\pi m_h^* kT}{h^3} \frac{p_x dp_x}{m_h^*} \ln \left\{1 + e^{\frac{\left(\frac{p_x^2}{2m_h^*} - E_F\right)}{kT}}\right\} \quad (4)$$

&

$$\boxed{N(\xi, E_x, T) = \frac{4\pi m_h^* kT}{h^3} \ln \left\{1 + e^{\frac{-(E_x + \xi)}{kT}}\right\} dE_x}$$

Where, $\xi = E_F - E_V$

Appendix-D

Taylor Series Expansion

Taylor series gives you the expansion of the given function around to a close point.

$$f(x+a)=f(x)+af'(x)+\frac{a^2}{2!}f''(x)+...$$

We have tunneling probability.

$$D(E_x)=\exp\left\{\frac{-4\pi}{h}\int_a^b\left[2m_h^*(qV(x)-E_x)\right]^{\frac{1}{2}}dx\right\}$$

or

$$\ln D(E_x)=\left\{\frac{-4\pi}{h}\int_a^b\left[2m_h^*(qV(x)-E_x)\right]^{\frac{1}{2}}dx\right\} \qquad (1)$$

So using Taylor series we can write, expand the R.H.S of equation (1) around the energy $\varepsilon_x=qV_b-E_x$ so we have.

$$f(E_x)=\left\{\frac{-4\pi}{h}\int_a^b\left[2m_h^*(qV(x)-E_x)\right]^{\frac{1}{2}}dx\right\}$$

Or
$$f(qV_b-\varepsilon_x)=\left\{\frac{-4\pi}{h}\int_a^b\left[2m_h^*(qV(x)-(qV_b-\varepsilon_x))\right]^{\frac{1}{2}}dx\right\} \qquad (2)$$

But according to Taylor series expansion equation (2) is given by ,

$$f(qV_b-\varepsilon_x)=f(qV_b)-f(qV_b)'\varepsilon_x+f(qV_b)''\varepsilon_x^2-..... \qquad (3)$$

Value of $f(qV_b)$ can be calculated by putting $qV_b \rightarrow qV_b + \varepsilon_x$ on both side of equation (2),

$$f(qV_b) = \left\{ \frac{-4\pi}{h} \int_a^b \left[2m_h^* (qV(x) - qV_b) \right]^{\frac{1}{2}} dx \right\}$$

To get $f(qV_b)'$ differentiating equation (2) w.r.t. qV_b & Again putting $qV_b \rightarrow qV_b + \varepsilon_x$ on both side of differentiation.

$$f(qV_b - \varepsilon_x)' = \left\{ \frac{2\pi}{h} \int_a^b \left[2m_h^* (qV(x) - (qV_b - \varepsilon_x)) \right]^{\frac{-1}{2}} dx \right\}$$

$$f(qV_b)' = \left\{ \frac{2\pi}{h} \int_a^b \left[2m_h^* (qV(x) - qV_b) \right]^{\frac{-1}{2}} dx \right\}$$

Similarly the second derivative can be calculated

$$f(qV_b)'' = \left\{ \frac{-\pi}{h} \int_a^b \left[2m_h^* (qV(x) - qV_b) \right]^{\frac{-3}{2}} dx \right\}$$

Now the equation (3) can be written as follows,

$$f(qV_b - \varepsilon_x) = -\left[b_1 + c_1 \varepsilon_x + f_1 \varepsilon_x^2 + \ldots\ldots \right]$$

Where b_1, c_1 & f_1 are given by,

$$b_1 = \left\{ \frac{4\pi}{h} \int_a^b \left[2m_h^* (qV(x) - qV_b) \right]^{\frac{1}{2}} dx \right\}$$

$$c_1 = \left\{ \frac{2\pi}{h} \int_a^b \left[2m_h^* (qV(x) - qV_b) \right]^{\frac{-1}{2}} dx \right\}$$

$$f_1 = \left\{ \frac{\pi}{h} \int_a^b \left[2m_h^* (qV(x) - qV_b) \right]^{\frac{-3}{2}} dx \right\}$$

So finally equation (1) is given by,

$\therefore$ $\ln D(E_x) = -[\, b_1 + c_1 \varepsilon_x + f_1 \varepsilon_x^2 + \ldots\ldots\ldots\ldots]$

or $D(E_x) = \exp -[\, b_1 + c_1 \varepsilon_x + f_1 \varepsilon_x^2 + \ldots\ldots\ldots\ldots]$

Appendix-E

Value of constants

$$b_1 = \left\{ \frac{4\pi}{h} \int_a^b \left[2m_h^* \left(qV(x) - qV_b \right) \right]^{\frac{1}{2}} dx \right\}$$

$$c_1 = \left\{ \frac{2\pi}{h} \int_a^b \left[2m_h^* \left(qV(x) - qV_b \right) \right]^{\frac{-1}{2}} dx \right\}$$

We have to solve b_1 & c_1 for carriers in the energy range $qV_b<E_x<q\phi$, so taking the value of $qV(x)$ from equation (13) we get .

$$\left.\begin{array}{ll} qV(x) = 0 & \text{for } |x| > W_{gb}/2 \\ qV(x) = q\phi & \text{for } |x| < W_{gb}/2 \end{array}\right\}$$

$$b_1 = \frac{4\pi}{h} \left(2m_h^* \right)^{1/2} \int_{-\frac{W_{gb}}{2}}^{\frac{W_{gb}}{2}} \left[q\phi - qV_b \right]^{1/2} dx$$

$$b_1 = \frac{4\pi}{h} \left(2m_h^* \right)^{1/2} \left[q\phi - qV_b \right]^{1/2} \int_{-\frac{W_{gb}}{2}}^{\frac{W_{gb}}{2}} dx$$

Which after solving and applying the limits gives

$$b_1 = \frac{4\pi}{h} W_{gb} \left(2m_h^* \right)^{1/2} \left(q\phi - qV_b \right)^{1/2}$$

Similarly the value of the c_1 can be calculated,

$$c_1 = \frac{2\pi}{h}\left(2m_h^*\right)^{1/2}\int_{x_1}^{x_2}\left[qV(x)-qV_b\right]^{\frac{-1}{2}}dx$$

$$c_1 = \frac{2\pi}{h}\left(2m_h^*\right)^{1/2}\int_{-\frac{W_{gb}}{2}}^{\frac{W_{gb}}{2}}\left[q\phi - qV_b\right]^{-1/2}dx$$

$$c_1 = \frac{2\pi}{h}\left(2m_h^*\right)^{1/2}\left[q\phi - qV_b\right]^{-1/2}\int_{-\frac{W_{gb}}{2}}^{\frac{W_{gb}}{2}}dx$$

so using this integral & putting the same limit we get the value of c_1.

$$\boxed{c_1 = \frac{2\pi}{h}W_{gb}\left(2m_h^*\right)^{1/2}\left(q\phi - qV_b\right)^{-1/2}}$$

Appendix-F

Current Density

$$I_1 = \left[\int_{qV_b+qV_{gb}/2}^{q\phi+qV_{gb}/2} \left\{ \exp\left[\frac{-\left(E_x+\xi-\frac{qV_{gb}}{2}-qV_L\right)}{kT} \right] \right\} \exp\left[-\left(b_1+c_1\varepsilon_x\right)\right] dE_x \right]$$

$$I_1 = e^{-\left(\xi-\frac{qV_b}{2}-qV_L\right)/kT} e^{-\left(b_1+c_1qV_b\right)} \int_{qV_b+qV_{gb}/2}^{q\phi+qV_{gb}/2} e^{\frac{-E_x(1-c_1kT)}{kT}} dE_x$$

$$I_1 = e^{-\left(\xi-\frac{qV_b}{2}-qV_L\right)/kT} e^{-\left(b_1+c_1qV_b\right)} \left[\frac{e^{-E_x(1-c_1kT)/kT}}{-\left(1-c_1kT\right)/kT} \right]_{qV_b+qV_{gb}/2}^{q\phi+qV_{gb}/2}$$

$$I_1 = \frac{kT}{\left(1-c_1kT\right)} e^{-\left(\xi-\frac{qV_b}{2}-qV_L\right)/kT} e^{-\left(b_1+c_1qV_b\right)} \left[e^{-\left(qV_b+qV_{gb}/2\right)\left(1-c_1kT\right)/kT} - e^{-\left(q\phi+\frac{qV_{gb}}{2}\right)\left(1-c_1kT\right)/kT} \right]$$

$$\boxed{I_1 = \frac{kT}{\left(1-c_1kT\right)} e^{-(\xi)/kT} e^{-\left(b_1+c_1qV_b\right)} e^{\frac{\left(qV_L+c_1kTqV_{gb}/2\right)}{kT}} \left[e^{-qV_b\left(1-c_1kT\right)/kT} - e^{-q\phi\left(1-c_1kT\right)/kT} \right]}$$

Similarly the second integral can be solved.

$$I_2 = \left[\int_{qV_b - qV_{gb}/2}^{q\phi - qV_{gb}/2} \left\{ \exp\left[\frac{-\left(E_x + \xi + \frac{qV_{gb}}{2} + qV_R \right)}{kT} \right] \right\} \exp[-(b_1 + c_1 \varepsilon_x)] dE_x \right]$$

$$\boxed{I_2 = \frac{kT}{(1 - c_1 kT)} e^{-\xi/kT} e^{-(b_1 + c_1 qV_b)} e^{\frac{-\left(qV_R + c_1 kT qV_{gb}/2 \right)}{kT}} \left[e^{-qV_b (1 - c_1 kT)/kT} - e^{-q\phi (1 - c_1 kT)/kT} \right]}$$

Appendix-G

Potential Across Grain Boundary

Writing the Poisson's Equation for the grain boundary region, we get,

$$\frac{d^2V(x)}{dx^2} = \frac{qN_G}{\varepsilon} \qquad \text{For } |x| < \frac{W_{gb}}{2} \tag{1}$$

Integrating and applying the boundary condition at $x = \frac{W_{gb}}{2}$, $V(x) = \phi$

$$\frac{dV(x)}{dx} = \frac{qN_G}{\varepsilon}\left(x - \frac{W_{gb}}{2}\right) \tag{2}$$

Further integrating and applying the boundary condition at $x = \frac{-W_{gb}}{2}, V(x) = \phi$

$$V(x) = \frac{qN_G}{2\varepsilon}\left(x - \frac{W_{gb}}{2}\right)^2 + \left(\phi - \frac{qN_G}{2\varepsilon}W_{gb}^2\right) \tag{3}$$

$$V(x = \frac{W_{gb}}{2}) = \phi - \frac{qN_G}{2\varepsilon}W_{gb}^2$$

$$V(x = -\frac{W_{gb}}{2}) = \phi$$

As V_d is half of the potential drop across the depletion region. It can be calculated by taking the difference of above two equations.

$$\therefore 2V_d = \frac{qN_G}{2\varepsilon}W_{gb}^2.$$

$$V_d = \frac{qW_{gb}^2 N_G}{4\varepsilon} \quad \text{or} \quad V_d = \frac{qQ_t^2}{4\varepsilon N_G} \cdot (\text{as } Q_t = W_{gb} N_G) \tag{4}$$

Now from the [23] dealing our grain boundary likes metal –semiconductor (Schottky barrier) problem. We can write the expression of total potential across semiconductor & at the interface of grain boundary.

$$V = V_s + V_i$$

$$V \approx 1 + \frac{W_{gb} q D_{ss}}{\varepsilon} V_s + \left(\frac{qN_G}{2\varepsilon}\right)^{\frac{1}{2}} \left[V_b^{1/2} - (V_b - V_L)^{\frac{1}{2}}\right] \tag{5a}$$

$$V \approx 1 + \frac{W_{gb} q D_{ss}}{\varepsilon} V_s + \left(\frac{qN_G}{2\varepsilon}\right)^{\frac{1}{2}} \left[V_b^{1/2} - (V_b + V_R)^{\frac{1}{2}}\right] \tag{5b}$$

where D_{ss} is the hole diffusivity in the silicon grain

Equation (5a) & (5b) represent the same potential ,so the potential across the grain boundary can be found by taking the difference of last term in the expressions (5a)& (5b) ,i.e. difference in potential at interface.

$$V_{gb} = \left(\frac{qN_G}{2\varepsilon}\right)^{\frac{1}{2}} \left[(V_b + V_R)^{\frac{1}{2}} - (V_b - V_L)^{\frac{1}{2}}\right] \tag{6}$$

Now as the applied voltage is very less as compare to barrier height ($V_0 << V_b$) $V_L = V_b$ And $V_R = 2V_d - V_b$ by [4], with these relation equation (6) changes to as follows. ,

$$V_{gb} = W_{gb} \left(\frac{qN_G}{2\varepsilon}\right)^{1/2} (2V_d)^{1/2} \tag{7}$$

So finally equation (4) and (7) give relation between potential across grain boundary and total potential drop across the depletion region.

$$\boxed{V_{gb} = W_{gb} \frac{N_G}{Q_t} 2V_d}$$

Appendix-H

Newton-Raphson Method

Let x_0 be an approximate value of a root of the equation $f(x)= 0$, and let x_0+h be the exact value of the corresponding root, where h is very small quantity. Then,

$$f(x_0+h)= 0 \qquad (1)$$

Since x_0+h is the root of the equation $f(x)= 0$.

Expanding (1) by Taylor's theorem, we get

$f(x_0+h) = f(x_0) + hf'(x_0) + h^2 f''(x_0)/2! +.....= 0$

Since h is very small, neglecting second and higher order terms and taking the first approximation, we have

$f(x_0) +hf'(x_0) = 0 \Rightarrow h =-f(x_0)/f'(x_0)$, provided $f'(x_0) \neq 0$.

$$\therefore x_1= x_0+h = x_0 - f(x_0)/f'(x_0) \qquad (2)$$

Relation (2) gives the improved value of the root over the previous one. Now substituting x_1 for x_0 and x_2 for x_1 in (2), we get

$$x_2 = x_1- f(x_1)/f'(x_1) \qquad (3)$$

In general, we can get an approximation or the iteration formula

$$\boxed{x_{n+1} = x_n - f(x_n)/f'(x_n)} \qquad (4)$$

From this formula, we can calculate successive better values of the root. Formula (4) is known as Newton-Raphson Method.

Bibliography

[1] Ted Kamins, Polycrystalline -silicon for Integrated Circuit Applications.

[2] J.Y.W. Seto, "The electrical properties of polycrystalline -silicon, " J. Appl. Phys., Vol. 46, p. 5247, 1975.

[3] G. Baccarani, B. Ricco, and G. Spadini, "Transport properties of poly crystalline silicon films, " J. Appl. Phys., Vol. 49, p.5565, 1978.

[4] Mohammad M.Mandurah, K.C .Saraswat. "A model for conduction in polycrystalline -silicon-part I " IEEE Vol .ED-28, NO.10 p.1163,oct 1981.

[5] G. J. Korsh and R.S Muller, "Conduction properties of light doped polycrystalline -silicon, " Solid-State Electron. Vol.21, p.1045, 1978.

[6] T. I. Kamins, "Hall Mobility in chemically deposited polycrystalline - silicon," J. Appl. Phys., Vol.42, p.1019, 1971.

[7] N. C. C. Lu, L. Gerzberg, and J. D. Meindl, "A quantitative model of the effect of grain size on the resistivity of polycrystalline -silicon resistors, " IEEE Electron Devices Lett, Vol.EDL-1, P.36, 1980.

[8] M. E. Cowher and T.O. Sedgwick, "Chemical vapor-deposited polycrystalline -silicon, "J. Electrochem. Soc, Vol.119, p.1565, 1978.

[9] L. Fripp And L. H. Slack, "Resistivity of doped polycrystalline -silicon films, " J. Electrochem. Soc., Vol.120, p.145, 1973.

[10] S. M. Sze "Physics of semiconductor Devices"(Interscience, New York).

[11] A.K. Ghatak "Quantum Mechanics".

[12] Eugen Merzbacher " Quantum Mechanics".(Third edition John Wiley & sons Inc.)

[13] C. Kittel, " Introduction to Solid Sate Physics".

[14] Sir Raiph, Howler, M.A, F. R. S & E. A. Guggenheim, M.A., Sc. D., F.R.S "Statistical thermodynamics."

[15] M. Taniguchi, M. Hirose, and Y. Osaka, "Subtitutional doping of chemically vapor-deposited amorphous silicon, " J. Cryst. Growth, Vol. 45, p. 126, 1978.

[16] J.C Knights, "Substitutional doping in amorphous semiconductors," Phil. Mag., Vol. 34, p. 663, 1979.

[17] J. G. Simmons, "Generalized formula for the electric tunneling effect between similar electrodes separated by a thin insulating film," J. Appl. Phys. , Vol.34, p.1793, 1983.

[18] M. M. Mandurah, K.C. Saraswat, C. R. Helms, And T. I. Kamins, "Dopant Segregation in polycrystalline -silicon, " J. Appl. Phys., Vol. 51, p. 5755, 1980.

[19] E. L. Murphy and R. H. Good, physical review, Vol. 102, Number 6, June 15, 1956 p.1464-1473.

[20] Nicky Chau-Chun Lu, IEEE Trans. ED, VOL. ED-30,NO.2 ,Feb 1983, pp. 137-149.

[21] Nicky Chau-Chun Lu, IEEE Trans. ED, VOL. ED-28,NO.7 ,July 1981, pp.818-830.

[22] G.Baccarani,M.improntra,B.Ricco "I-V characteristics of polycrystalline -silicon resistors. De Physique ,December 13 1978, pp.777

[23] R. Stratton "Voltage-current characteristics for tunneling through insulating films, " J. phys. chem. solids, Vol. 33, p. 1177, 1962.

[24] J.Martinez, J.Piqueras," On the mobility of polycrysttaline semiconductor", Solid-State Electronics Vol.23, pp 297-303

[25] T. I. Kamins, J. Appl. Phys. Vol.42, p. 4357, 1971.

[26] H. J. Queisser, K. Hubner, Phys. Rev. Vol.123, p. 1245, 1980.

[27] S.J. Fonash, "The role of the interfacial layer in metal–semiconductor solar cells", J. Appl. Phys., Vol.46, p. 1286, 1975.

[28] M. M. Mandurah, "The physical and electrical properties of polycrystalline -silicon" J. Appl. Phys., Vol.45, p. 1243, 1981.

[29] F. Mansour, M. Bouchermat, M. Boukezzata, N. H. Touidjen, D. Bielle Daspet, K. Mirouh. "Conductivity of Boron-Implanted polycrystalline thin silicon films" Thin solid Films. Vol.261, p.12-17, 1995.

[30] D. M. Kim and F. Qian, IEEE Trans. Electron Dev., vol. ED-34 (8), p.1774, 1987

[31] M. Y. Channam and R. W. Dutton. J. Appl. Phys., vol. 52(15), p. 1222, 1988.

[32] N.C.C. Lu and C.Y.Lu, J. Electrochem. Soc., p.897 ,1984

[33] C. Y. Lu and N. S. Tsai, J. Appl. Phys., Vol. 59, p. 3574, 1986.

[34] Y. Wada and S. Nishimatsu, "grain-growth mechanism of heavily phosphorous-implanted polycrystalline -silicon," J. Electrochem. Soc., Vol. 125, p. 1499, 1978.

[35] K. Board and M. Darwish, J. Appl. Phys., Vol. 51, p. 4546, 1980.

[36] Len Mei, Michel Rivier, Young Kwark, and Robert W. Dutton, J. Electrochem. Soc., Vol. 129, No. 8, p. 1791, 1982.

[37] H. -J. Kim and C. V. Thompson, Appl. Phys. Lett., Vol. 48 (6), p. 399, 1986.

[38] L. R. Zheng, L. S. Hung, and J. W. Mayer, Appl. Phys. Lett., Vol. 51 (25), p. 2139, 1987.

[39] K.H.Gundlach and J.G. Simmons, "Range of validity of the WKB tunnel probability and comparison of experimental data and theory," Thin Solid Films, Vol.4,pp 61-79,1969.